nature biomedical engineering

REVIEW ARTICLE

https://doi.org/10.1038/s41551-021-00683-3

Wireless and battery-free technologies for neuroengineering

Sang Min Won[1,14], Le Cai[2,14], Philipp Gutruf[2,3,4] ✉ and John A. Rogers[5,6,7,8,9,10,11,12,13] ✉

Tethered and battery-powered devices that interface with neural tissues can restrict natural motions and prevent social interactions in animal models, thereby limiting the utility of these devices in behavioural neuroscience research. In this Review Article, we discuss recent progress in the development of miniaturized and ultralightweight devices as neuroengineering platforms that are wireless, battery-free and fully implantable, with capabilities that match or exceed those of wired or battery-powered alternatives. Such classes of advanced neural interfaces with optical, electrical or fluidic functionality can also combine recording and stimulation modalities for closed-loop applications in basic studies or in the practical treatment of abnormal physiological processes.

Advances in electronic, optoelectronic and microfluidic interfaces with living biosystems serve as foundations for versatile devices capable of interrogating and modulating the behaviour of the central and peripheral nervous systems[1–5]. Beyond their use in fundamental research, interfaces to neural tissues are also being developed as treatments of neurological disorders and diseases[6–11]. As with cochlear implants and cardiac pacemakers, the most advanced devices for human use exploit rigid and relatively large electronic modules electrically connected to metal electrodes as interfaces to collections of neurons. These systems and others, such as those for deep brain stimulation, can monitor and ameliorate diverse neurological disorders and diseases—in particular, depression, epilepsy, chronic pain, deafness and Parkinson's disease. Their limited modalities of operation and their mechanical mismatch with soft neural tissues can hinder long-term functionality and restrict anatomical applicability. Advances in neuroengineering can facilitate the development of long-lived neural interfaces with diverse operational modes and points of integrating in freely behaving animal models.

Recent progress in implantable neural interfaces has qualitatively extended the designs and capabilities of existing miniaturized systems to support the delivery of user-programmed optical[12–15], chemical[14,16–19] and electrical stimuli[20–23] in real time. Certain devices have formats that require only minimally invasive implantation procedures and offer operational stability over extended time periods. Such technologies are distinct from and potentially complementary to recently developed material-based approaches, such as nonlinear optical nanoparticles that convert incident near-infrared illumination into visible light[1,24,25], magnetic nanoparticles that transduce magnetic fields to mechanical, electrical and thermal stimuli[1,26–28], and contrast agents that enable ultrasound-induced transient opening of the blood–brain barrier for the local delivery of therapeutics[29,30]. In this Review Article, we discuss engineered miniaturized systems that exploit schemes in wireless power transfer, communication and digital control to support applications in neuroscience research and more generally in the monitoring of broad types of physiological processes[31–33].

Commonly used technologies for such applications rely on electrochemical power sources (such as batteries and supercapacitors) or on similarly large and bulky systems for energy harvesting[16,34–39] partly because of the technological maturity and widespread availability of the associated hardware. Conventional rigid printed circuit boards typically serve as mounting sites for centimetre-scale electronic components for wireless data transmission, for physiological recording and for the control of stimulation. Devices that use these designs can, however, cause irritation, infections and motion artefacts and they reduce freedom of motion, particularly in small animals. The size and weight of such systems represent key limiting features[40–44]. Large form factors also affect the precise interpretation of experimental data and often preclude behavioural studies in naturalistic environments. Instead, fully wireless and lightweight systems that are battery-free and adopt millimetre-scale dimensions, for complete and long-term implantation, enable continuous behavioural studies without the need for human interactions that can alter natural behaviours.

Here, we provide an overview of the latest technologies in such classes of wireless implantable devices and compare their designs and capabilities with those of tethered and battery-powered systems. We discuss materials selections and engineering approaches for the development of functional interfaces in the context of biocompatibility and hermeticity, wireless data communication and wireless power transfer. Although we highlight the use of these technologies for fundamental neuroscience research and for multifunctional neuroengineering in small animals, these same platforms also establish strategies and methods for devices that can be used in large animals and humans.

[1]Department of Electrical and Computer Engineering, Sungkyunkwan University, Suwon, South Korea. [2]Biomedical Engineering, College of Engineering, The University of Arizona, Tucson, AZ, USA. [3]Bio5 Institute and Neuroscience GIDP, University of Arizona, Tucson, AZ, USA. [4]Department of Electrical and Computer Engineering, University of Arizona, Tucson, AZ, USA. [5]Department of Materials Science and Engineering, Northwestern University, Evanston, IL, USA. [6]Center for Bio-Integrated Electronics, Northwestern University, Evanston, IL, USA. [7]Department of Biomedical Engineering, Northwestern University, Evanston, IL, USA. [8]Center for Advanced Molecular Imaging, Northwestern University, Evanston, IL, USA. [9]Department of Mechanical Engineering, Northwestern University, Evanston, IL, USA. [10]Department of Chemistry, Northwestern University, Evanston, IL, USA. [11]Department of Neurological Surgery, Northwestern University, Evanston, IL, USA. [12]Department of Electrical and Computer Engineering, Northwestern University, Evanston, IL, USA. [13]Simpson Querrey Institute for BioNanotechnology, Northwestern University, Evanston, IL, USA. [14]These authors contributed equally: Sang Min Won, Le Cai. ✉e-mail: pgutruf@arizona.edu; jrogers@northwestern.edu

Limitations of tethered systems

Technologies that rely on physical tethers—such as electrical wires, optical-fibre cables or fluidic tubing—to external supporting hardware are commonly used in neuroscience research and in medical systems, in part owing to the simplicity and commerical availability of the component parts. For example, optogenetic stimulation and photometric recordings for the interrogation of neural function in the brain typically use optical-fibre technologies adapted from those used by the telecommunications industry[45,46]. The fibre connects to an external light source and creates an optical interface with a targeted region in the brain. The materials and geometric properties of the fibre and coupling of the light source determine the illumination[47–51]. Examples include angle-adjusted optical coupling to tapered fibres for selective neurostimulation[47], multifunctional fibres with integrated conductive filaments for coordinated electrical recording, optogenetic stimulation combined with fluidic channels for delivery of a biologic agent[48], and fibre-based photometers for the stimulation and recording of fluorescence from genetically targeted Ca^{2+} indicators[49,50,52] and fluorescent voltage reporters[51]. Other tethered systems use head-mounted electronics or cable assemblies (or both) in conjunction with implantable light sources and electrical or optical recording components. For instance, advanced systems use microstructured injectable needles with integrated microscale inorganic light-emitting diodes (μ-ILEDs) and electrodes for multisite recording and stimulation with spatial resolution on the cellular scale[53]. Other approaches use miniaturized head-stage camera set-ups coupled with chronically implanted lenses for visualizing neural circuit dynamics with high spatial resolution[54,55].

However, such tether-based technologies pose particular difficulties when interfacing with highly mobile body areas such as the spinal cord and peripheral nerves because of the need for fixation to mechanically stable parts of the anatomy (such as the skull) or to specialized orthoses[56]. Furthermore, the forces exerted on the implant by the tethers during natural motions, and those associated with the plugging, unplugging and unwinding of the cables, result in micrometre-scale motions between the rigid probes and the soft tissues. These effects can cause tissue damage and artefacts that lead to reduced chronic stability and signal fidelity[57,58]. Also, particularly for advanced interfaces that demand multichannel operation[59], unrestrained animals often attempt to remove or disconnect the cables.

Wireless implantable devices for recording and stimulation can offer robust, long-lasting and high-fidelity interfaces with the central and peripheral nervous systems. These platforms enhance experimental reproducibility and reduce interactions with the test subjects and with environmental obstacles (Fig. 1a). The advantages of wireless implants become apparent in comparative studies of fibre-tethered and battery-powered wireless optogenetic photometric devices. The data show that the tethers can, in many cases, significantly impede social behaviours and the overall patterns of activity of the animals[60] (Fig. 1b,c). In one set of experiments that compared mice bearing tethered or untethered devices, animals with fibre-based photometers exhibited reduced social interactions (14 s versus ~21 s) and total activity (~75 m versus ~100 m), with less time spent in the centre of the experimental enclosure (~30 s versus ~70 s). These behaviours are consistent with increased levels of anxiety[60]. Such results suggest that wireless approaches can significantly improve the validity of animal studies by minimizing the effects of the devices on motion. The wireless system used in the study in ref. [60] also reduced the requirements for supporting equipment and interface hardware, thereby decreasing the overall cost of the system to less than US$100, roughly twenty times less than the typical cost of a fibre-based photometry system. Similar considerations in costs and constraints apply to recording and modulation schemes based on electrical and fluidic approaches[61,62].

Electrophysiological recordings from cortices of bats during social engagements indicate that correlated neural activities develop across the brains of the animals[63]. Vocalization-correlated neural signals frequently occur and in manifold forms in unrestrained animals in social groups[64]. Studies of unrestrained animals also indicate neuromodulatory therapeutic outcomes that are difficult to observe in restrained test subjects. For example, in a mouse model of autism, stimulating neurons in the right crus rescued social impairments, suggesting a therapeutic potential of cerebellar neuromodulation in autism spectrum disorders[65].

Current tethered systems present additional challenges for use with non-human primates and other animal models that are more dexterous and possess greater physical strength than rodents[64]. Emerging interest in the characterization of generalizable aspects of the central and peripheral nervous systems has led to increased research focus on the study of animal models other than rodents. However, the use of tethered systems in fish[66,67], bats[68], birds[69], monkeys[64] and other animals (Fig. 1d) is particularly difficult, thereby leading to limitations in the diversity of animal subjects that can be studied effectively. Although certain devices with implantable microscale probes for recording and stimulation can be made fully wireless by using head stages to house battery packs and electronics[59,70–72], the use of percutaneous connections exposes the animals to risks of infection and requires the recharging or replacement of batteries and hence frequent human interactions.

Design considerations for fully implantable devices

Mechanical and biochemical forms of mismatch at biotic–abiotic interfaces can cause insertion-related trauma and chronic inflammation in host neural tissues[73,74]. In many cases, foreign-body responses can degrade the sensitivity and stimulation efficiency of the biointerfaces[75,76]. Engineering approaches that minimize these effects demand combined attention to mechanics[77], materials[73] and physical form factors[78]. In particular, the mechanical characteristics of implants play crucial roles in the onset of foreign-body reactions[79]. In fact, owing to device motion in relation to the interfaced soft tissues, devices with high stiffnesses tend to induce large insertion-related lesions[16,60,80], increased inflammation reactions and neuronal apoptosis[57,58]. Soft neural interfaces can be achieved with devices that offer materials or system-level mechanical compliance. The resulting technologies can allow minimally disruptive integration and intimate interfaces with various parts of the central and peripheral nervous systems at anatomically complex and dynamic locations[3,73,81,82]. Devices with mechanical properties close to those of tissues can be realized by using soft materials[83] or hybrid constructs of stiff materials and soft supports[84], such as conjugated polymers[85,86], carbon nanomaterials[87,88], buckled nanoribbons[89], serpentine nanowires[90] and mesh structures[91] of metals and semiconductors. The supporting materials and encapsulants often determine the effective mechanical properties of the devices. Hence, flexible substrates, often made of polyimide[86] or parylene[92], and stretchable substrates, typically made of polydimethylsiloxane (PDMS)[77], are of particular interest. Conformal surface-mounting sheets[93–97] or soft penetrating probes[60,98–100] can be used to build soft neural interfaces for recording physiological signals and for delivering neural stimuli[1,3].

Wireless and fully implantable systems also require mechanically compliant electronic components for control, power harvesting and data communication[95,96,98,100–102]. Serpentine metal traces with shapes that ensure high conductivity under tensile strains of up to 300% (ref. [103]) can be used in structured antennas and interconnects to provide reliable operation for strains that exceed those set by natural biological motions (less than 20–50%)[98,104,105]. In systems that demand active electronics, off-the-shelf components such as microcontrollers and radio units are attractive because of their commercial availability and low cost. When assembled on

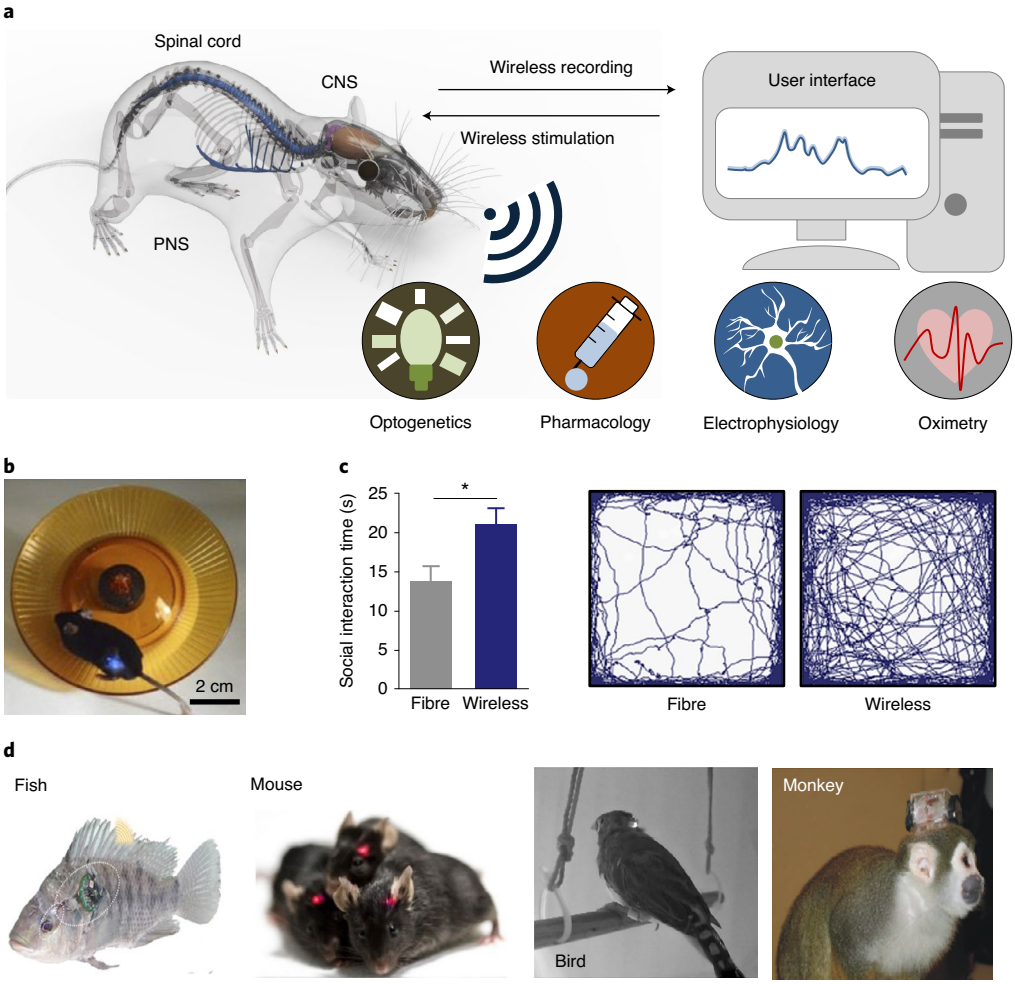

Fig. 1 | Implanted wireless electronics. a, Fully implantable wireless interfaces for the central nervous system (CNS), spinal cord and peripheral nervous system (PNS) can offer functional options for electronic or optogenetic recording and stimulation and for microfluidic drug delivery. **b**, A mouse with a wireless device implanted in the sciatic nerve running on a wheel. **c**, Direct experimental data from wireless and tethered (fibre) electronic implants highlight the advantages of the former in the study of social interactions and total activity levels of mice in open-field arenas. **d**, Examples of miniaturized wireless implantable electronic systems for in vivo physiological recording and neural stimulation in fish, mice, birds and monkeys. Figure reproduced with permission from: **b**, ref. [98], Springer Nature America, Inc.; **c**, ref. [60], National Academy of Sciences; **d**, fish image, ref. [67], Elsevier; **d**, monkey image, ref. [64] Elsevier. Rat in **a** adapted from leo3Dmodels / Turbosquid.

flexible and stretchable substrates with serpentine interconnects[96] and strain-isolating mechanical designs[95], the resulting systems can support device-level deformability to levels that can meet demanding requirements[95,96,102].

With the exception of temporary implants based on bioresorbable materials[106], most devices require isolation from biofluids to avoid electrical shorting and ionic contamination of the functional elements during extended operational periods[107]. Material choices for isolation barriers must meet requirements in biocompatibility and in water and ion permeabilities[108]. Optogenetic stimulators encapsulated by biocompatible bilayers of parylene and PDMS[109], for example, can operate during immersion in physiological saline solution at 60 °C for at least 90 days—which corresponds to projected lifetimes of up to a year at 37 °C (ref. [100])—without degradation in mechanical flexibility or functionality[102]. Inorganic materials such as ceramics and metals offer higher levels of hermeticity than polymers[110]. Physically transferred layers of silicon dioxide (thicknesses of ~1 μm) grown thermally on silicon wafers act as barriers to biofluids and provide stability for potentially many decades (over 70 years) in simulated physiological conditions[111]. Additional capping layers (hafnium dioxide, for example) can further enhance the long-term stability of the devices by reducing the transport of ions and by slowing the rates of hydrolysis. Reference [112] provides additional details on biofluid-isolation barriers for bioelectronic systems that support long-term stable operation.

Power sources and wireless communication

Conventional small and lightweight batteries can satisfy the power requirements for wireless devices with sophisticated function, as shown with optoelectronic photometers for monitoring neuronal dynamics in the deep brain[60] and with optofluidic systems for programmable pharmacology and optogenetics[16]. However, batteries with sufficient storage capacity for many practical applications have sizes larger than 3 cm^3 and weigh more than 2 g (ref. [71]), and hence require percutaneous wiring when used in small animals[113]. Moreover, battery recharging disrupts the continuity of experiments and can affect the behaviour of the animals[114]. Batteries often occupy up to 90% of the volume of implantable devices[115] and account for more than 60% of their weight[60]. Reducing the sizes and masses of the batteries, or completely eliminating them, provides significant advantages, especially for devices fabricated on thin polymeric substrates[98,102].

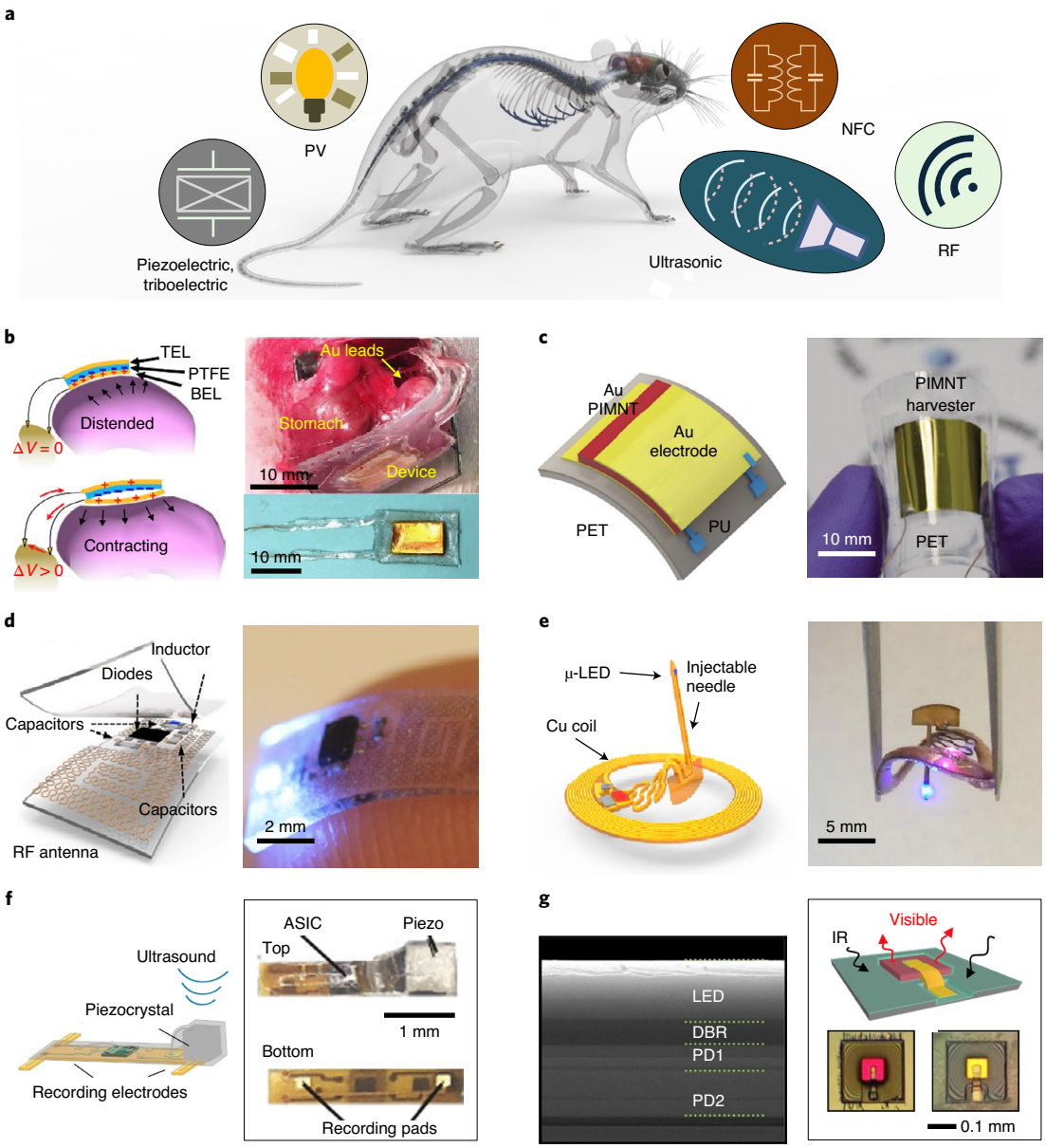

Fig. 2 | Strategies for supplying power to wireless and battery-free implantable devices. a, Power harvesting and delivery strategies include electromechanical (piezoelectric and triboelectric), photovoltaic (PV), magnetic resonant coupling (near-field), RF power transfer (far-field) and ultrasonic transduction. **b**, Example of a device for providing electrical stimulation to the vagus nerve for weight control, with the power supplied by a triboelectric generator that harvests mechanical energy from movements of the stomach. *V*, voltage; BEL, bottom electrode layer; PTFE, polytetrafluoroethylene; TEL, top electrode layer. **c**, A flexible piezoelectric energy harvester for powering a deep-brain stimulator. PET, polyethylene terephthalate; PIMNT, $Pb(In_{1/2}Nb_{1/2})O_3$-$Pb(Mg_{1/3}Nb_{2/3})O_3$-$PbTiO_3$; PU, polyurethane. **d**, A soft, stretchable and fully implantable wireless optogenetic stimulator powered by far-field RF power transfer. **e**, A fully implantable wireless optogenetic deep-brain stimulator powered by magnetic resonant coupling. **f**, A device for electrophysiological recording powered by ultrasound. **g**, An implantable microscale optoelectronic neuromodulator powered by infrared (IR) light. DBR, distributed Bragg reflector; PD1 and PD2, photovoltaic diodes. Figure reproduced with permission from: **b**, ref. [119], Springer Nature Ltd; **c**, ref. [118], Royal Society of Chemistry; **d**, ref. [98], Springer Nature America, Inc.; **e**, ref. [100], Cell Press; **f**, ref. [126], Cell Press; **g**, ref. [124], National Academy of Sciences. Rat in **a** adapted from leo3Dmodels / Turbosquid.

Schemes for wireless delivery of power can enable devices with lightweight, miniaturized form factors with unlimited operational lifetimes[116,117] (Fig. 2a). Options include body-generated power (such as kinetic energy harvested from skeletal[118] and visceral motions[119], chemical energy from blood sugar[120] and thermal energy from body heat[121]) or external power transmitted via radio-frequency (RF) electromagnetic fields[100,101,122], light illumination[123,124] or ultrasonic waves[125,126] (Table 1). Power supplied with such schemes must meet system-dependent power-consumption requirements. For example, electrophysiological recordings based on optimized application-specific integrated circuits (ASICs) can consume as low as a few microwatts per channel[34,127–130], whereas photometric recordings typically require average powers in the range of milliwatts[131]. Even with a given operation modality, power consumption may differ depending on implant location[100,119,122,132] (Table 2).

Power derived from internal biological sources (such as electromechanical[119,133,134], biochemical[135,136], bioelectrical[137,138] and thermal

Table 1 | Summary of device architectures for the wireless and battery-free operation of fully implantable stimulation and recording systems for the central nervous system

Power source		Features	Example	Reference
External power source				
Electromagnetic	Far-field, passive	Weight: 16–33 mg Available power: ~3–5 mW Operational distance: 0.1–3 m Tissue impact: SAR 6,150–6,169 mW kg^{-1}	Downlink: RF Uplink: N/A Control: analog, multiband receiving antenna Embodiment: subdermal Applications: deep-brain stimulation, spinal-cord stimulation or peripheral neural stimulation	98,101,122
	Near-to-mid field, magnetic resonant coupling	Weight: ~30 mg Available power: ~5–10 mW Operational distance: 0.1–1 m Tissue impact: SAR < 20 mW kg^{-1} (approximately)	Downlink: RF Uplink: N/A Control: digital, active Embodiment: subdermal Applications: brain optogenetics, local oximetry, microfluidic drug delivery	100,102, 145,192
			Downlink: RF, Bluetooth Uplink: Bluetooth Control: closed-loop Embodiment: on organ or nerve Applications: physiological recording, peripheral neural stimulation	141
	Photovoltaic	Weight: 11 μg to 70 mg Available power: 45 μW to 7 mW Operational distance: ~0.5 m Tissue impact: heating of 5 °C with 250–300 mW mm^{-2} IR radiation for 20 min	Downlink: light (green) Uplink: light (red) Control: digital Embodiment: N/A Applications: brain neural recording	123,124, 142,158
Ultrasonic		Weight: 7.6 mg Available power: 0.12 mW Operational distance: ~10 cm in tissue, direct body–transducer contact Tissue impact: ultrasonic attenuation ~0.8–1.48 dB cm^{-1} (soft tissue); ~40–60 dB cm^{-1} (bone); ~80–120 dB cm^{-1} (lung)	Downlink: ultrasonic Uplink: ultrasonic Control: N/A Embodiment: deep in tissue or on nerve Applications: physiological or neural recording	125,126,184
Internal power source				
Triboelectric		Available power: ~0.26 mW (peak) Operational distance: N/A	Downlink: N/A Uplink: N/A Control: N/A Embodiment: on organ or nerve Applications: self-triggered electrical neural stimulation	118,119,134
Biofuel		Available power: ~μW Operational distance: N/A Tissue impact: biofouling, inflammation	Downlink: N/A Uplink: Bluetooth Control: digital Embodiment: N/A Applications: implantable biofuel cell	136,149

N/A, not applicable.

forms of energy[139]) can enable self-contained fully autonomous operation[116,140]. However, the relatively low output power available from these sources limits applications to narrow classes of systems that do not require advanced control electronics or radios, such as simple interfaces for cardiac pacing and pulsatile neurostimulation[119,134]. Additionally, the intermittency and physiological load associated with power derived from biological processes may affect the reliable operation of the implants and the health of the host organism. By contrast, external power sources, including those that rely on RF radiation[98,122], magnetic resonant coupling[100,141], illumination[124,142] or ultrasonic waves[125,126], decouple the device operation from the subject and can therefore provide a reliable and constant power supply for multimodal physiological recording[131,143], optofluidic neuromodulation[62,144] or closed-loop regulation of organ functions[141]. Depending on the harvesting mode, externally powered systems fall into two categories. The first involves far-field RF radiation[98] or near-field magnetic resonant coupling[100], whereby the wireless power link connects to transmitters installed on or around the cage of the animal[145]. The RF waves or magnetic fields fill the entire test space or may selectively couple to an animal[122] independent of its location[102]. The second category includes imaging set-ups for optical illumination[123], direct body contacts for ultrasound[126]

Table 2 | Power consumption for the various modalities for neural recording and stimulation

Modality of operation	Power consumption
Electrical recording	9 μW per channel[127], 3.37 μW per channel[128], 16 nW (ref. [129]), 906 μW per channel[34], 8 μW per channel[61], 2 mW per channel[130]
Optical recording	10 mW (peak) and 2 mW (average)[143], 10.37 mW (active) and 119 μW (sleep)[131], <15 mW (continuous)[60]
Electrical stimulation	21.4 mW (peak), 1.8 mW (average) (30 Hz, 0.8% duty cycle)[132], <40 μW (ref. [119])
Optogenetic stimulation	2–10 mW (continuous mode, depending on light intensity)[100,122]
Pharmacological stimulation	1.3 mW (average, 86.5% duty cycled)[62]

or proximity antennas for inductive coupling between transmitting and receiving coils[146]. Although these schemes can be realized in devices with submillimetre dimensions[123,124,146], they cannot be easily configured to operate across an entire test space; hence, they can impose constraints on experiments that involve freely moving animals[123,124,146].

Internal power harvesting. Piezoelectric and triboelectric effects allow conversion of the kinetic energy of voluntary (skeletal) and autonomic muscular motions (cardiovascular, respiratory and gastrointestinal) into electrical energy[117,119,133,134,147]. They can allow for autonomous device operation without the need for separate power supplies[140]. In one example, a flexible triboelectric nanogenerator for weight control generates biphasic pulses of electrical current in response to peristalsis of the stomach[119], stimulating the vagal afferent fibres to reduce food intake (Fig. 2b). In another case, bending of a flexible piezoelectric device creates a pulsed electric current to stimulate the motor cortex of mice (Fig. 2c), thereby acting as a self-powered device for deep-brain stimulation[118]. In that study[118], the extracorporeal piezoelectric generator connects to the stimulation probe via copper wires, and a linear stage creates the necessary cyclic bending deformations.

Control electronics with sufficient energy efficiency and components with continuous and predictable harvesting capabilities are essential for fully implantable systems, of the type considered here. The primary disadvantages of electromechanical-energy-scavenging technologies are the limited amount of available power and their pulsatile (often intermittent) nature[116]. Most devices that depend on skeletal motion generate peak powers of less than 1 mW, with low duty cycles and considerable reductions after rectification[118]. Power levels in the range of tens of microwatts (power density of ~11 μW cm^{-2}) can be expected from visceral motions[119,133], which, even in conjunction with capacitors or other components for energy storage, is typically insufficient for microcontrollers[102], optoelectronic devices[60], microfluidic actuators[16] and wireless communication systems. Therefore, existing piezoelectric and triboelectric generators are mostly relevant for use in passive devices with simple functions, such as the production of pulsed voltages in pacemakers and of instantaneous neural stimulation (which require peak powers of tens of microwatts[133,134,148]).

Other forms of energy scavenging include biofuel cells[120,136,149,150] and thermoelectric generators[121,133]. Such options are of interest because the corresponding energy sources (such as glucose, oxygen or thermal gradients) are always present in living organisms. However, they have modest power outputs. For instance, normal temperature gradients between the skin and ambient air (~10 K; ref. [121]) provide a thermoelectric power of only ~28.5 μW cm^{-2}. The output power of biofuel cells falls within a similar range (~10 μW cm^{-2}; refs. [135,151]). Nevertheless, research efforts on implantable biofuel cells in a range of host organisms (for example, insects[152], snails[153], rats[154] and rabbits[149]) suggest some promise. A recent study[149] demonstrated the wireless operation of enzymatic biofuel cells implanted in freely behaving rabbits, whereby battery-powered Bluetooth-based modules controlled and monitored the performance of the cells (Table 1). These systems yielded powers of ~1.6 μW cm^{-2} (estimated from a biocathode and bioanode with thicknesses of ~1 mm) for 30 min each day over 16 consecutive days, followed by reductions over 60 days of implantation. Device degradation followed mainly from inflammatory reactions, biofouling and degradation of the biocatalysts[135,155]. The effects of continuous internal power harvesting on the target organism require further investigation[155].

External power transmission. Dedicated power-delivery schemes based on transmission via electromagnetic radiation, acoustic vibrations or other means are often attractive as they outperform power-scavenging schemes in the amount and stability of the output power[116,140]. Significant amounts of power (up to ~500 mW)[156] can be reliably transmitted, with versatile design and deployment options. The main categories of remote power-transmission technologies include far-field RF, near-field magnetic resonant coupling, photonic power delivery and ultrasound transduction.

Far-field RF power transfer. RF radiation (frequency of 420 MHz at ~2.4 GHz and wavelengths of 0.1–1 m) emitted by a transmission antenna can be captured by a harvesting antenna and converted by a rectification circuit into direct current to drive the electronics[157]. Transmission can occur over long distances (up to many metres) and, with specialized primary antenna designs, uniform and continuous power delivery can be achieved throughout typical experimental arenas (~30 × 30 cm)[98]. Concepts in stretchable electronics[96] can be leveraged to create mechanically soft antennas and rectifying circuits in fully implantable miniaturized optoelectronic systems for optogenetic modulation of the spinal cord and of peripheral nerves[98] (Fig. 2d). In these reported examples, the antennas (~3 × 3 mm in size) harvest RF power through capacitive coupling between adjacent serpentine traces, thereby enabling compact and lightweight devices (overall size of ~0.7 × 3.8 × 6 mm and overall weight of ~16 mg) with low-modulus system-level mechanics (effective modulus of ~1.7 MPa) that are capable of accommodating irregular anatomical shapes and natural motions. Advanced antenna designs allow for multimodal operation, whereby spatially separated μ-ILEDs with multiple emission wavelengths (540 nm and 465 nm) can be independently powered by multiple antennas that resonate at distinct frequencies[101]. Active motion-tracking primary antenna arrays can localize power delivery to improve the harvesting efficiency. Given an input RF power of 2 W across a cage of 25 × 25 cm, μ-ILEDs for optogenetic stimulation can be activated while the animal is freely moving at an irradiance of 10 mW mm^{-2}, which corresponds to a power density of ~1.42–2.88 mW cm^{-2} (refs. [98,101]).

A disadvantage of far-field transmission is the strong dependence of the efficiency on the angle between the transmission and receiving antennas. This dependence is due to the trade-off between angular acceptance and antenna gain, in which high gain is often required to cast sufficient power[158]. As a result, considerable efforts in antenna designs[159] and transmitter-deployment strategies[101] are required to achieve reliable power harvesting. Additionally, RF transmission, especially at higher frequencies (1–4 GHz), can be affected by interference caused by environmental obstructions. In particular, conductive objects such as metals can nearly completely reflect RF waves in the relevant frequency range (0.5–4 GHz), and

dielectric materials with high refractive index can also create substantial reflections[160]. The interference between incoming RF waves and the reflected or scattered waves results in spatially varying RF power densities in the test space[160] and, in extreme cases, in the formation of hotspots and dead zones, which lead to potentially high specific absorption rates (SARs) and to lack of power supply, respectively.

One strategy to overcome these issues exploits an RF cavity that resonantly excites electromagnetic fields in the body of the animal, thus enabling a self-tracking operation, albeit with relatively high SAR levels (up to ~6.2 W kg^{-1})[122,161]. These high SAR values are due to strong power absorption by moisture and biological tissues at these RF frequencies, which in some cases leads to levels of heating that can alter essential biological activities[162]. Absorption is a particular concern for power-harvesting efficiency associated with fully implanted devices. This effect limits the amount of power that can be delivered without adverse biological effects.

Near-field wireless power transfer. First demonstrated by Nikola Tesla[163,164], near-field power transfer exploits non-radiative electromagnetic energy (within ~$\lambda/2\pi$ from the transmitter) and relies on inductive coupling between a transmitting coil and a receiving coil[165]. This scheme offers efficient power transmission over short distances, thereby enabling commercial solutions for the wireless charging of electric vehicles[166,167] and consumer electronics[168]. Nonetheless, the high sensitivity to axial and angular alignments between coils and a limited transfer range (less than a few centimetres) can create challenges for implantable devices[165]. The power-transfer efficiency and distance can be significantly improved by adopting transmitting and receiving resonators that are tuned to create strong magnetic resonant coupling[169,170]. Efficient power transfer can be achieved with high quality factor (Q-factor) resonators over large distances (up to a few metres)[169,170]. As a consequence of its non-radiative nature, magnetic resonant coupling, with frequencies ranging from ~100 kHz (refs. [171,172]) to ~200 MHz (ref. [173]), is relatively insensitive to changes in dielectric environments and to the presence of obstacles. Successful power transfer is possible in cases where the line of sight between the two resonators is completely obstructed[169], in complex surroundings, without dead zones and hotspots. Low frequencies used in implantable applications involve reduced tissue absorption[162] and therefore offer large penetration depths with minimal adverse biological effects, albeit with the requirement for larger receiving coils. High frequencies can support improved device efficiency[169] and reduced size[174].

In practical applications, 13.56 MHz (wavelength of ~12 m) represents an attractive choice of frequency because its absorption by biological tissues lies within an acceptable range[175] (Table 1) and because it aligns with standards in RF identification and near-field communication (NFC)[104]. In addition, communication can be implemented along with power transfer at the same carrier frequency to allow for wireless control and data transmission using NFC protocols[176,177]. Magnetic resonant coupling at 13.56 MHz for advanced classes of wearable and implantable electronics[178,179] occurs between two resonant systems: a primary coil enclosing a test arena and a secondary coil powering the implant[100,102,104,143]. In these experimental set-ups, the power-transfer efficiency weakly depends on the orientation and location of the secondary coils[180]. Consequently, reliable power harvesting (up to 12 mW for small rodent-sized devices[143]) with ~13 mW cm^{-2} can be achieved throughout a desired cage volume (determined by the size of the primary coil and the RF power source), and complex test environments can be addressed with simple antenna designs or deployment strategies[102]. With on-board circuits and electronic components encircled by the secondary coil, devices with miniaturized form factors (diameters of ~5 mm and weights of ~16 mg) are possible in encapsulated constructs that are biocompatible and chronically stable[102]. Magnetic resonant coupling depends on the magnetic flux captured by the secondary coil, with minimal sensitivity to its detailed shape. As a result, the overall device geometry can be easily adapted to accommodate various anatomical structures and the dynamic nature of biological tissues. In addition, fabrication methods compatible with well-established flexible printed-circuit-board technologies and with off-the-shelf components ensure standardized and scalable manufacturing and facilitate broad dissemination[102].

Another advantage of magnetic resonant coupling is its low SAR[175], which follows from the approximate power-law relationship of this quantity with relatively low frequencies (from hundreds of kHz to tens of MHz; ref. [165]) used in magnetic resonant coupling. This feature minimizes safety concerns during long-term operation and has consequently facilitated its implementation in a wide range of wireless, battery-free and fully implantable devices for localized tissue oximetry[143], for bioresorbable monitoring of intracranial pressure and temperature[106], for optogenetic stimulation in the central and peripheral nervous systems and for pharmacological modulation[100,144]. A subdermally implantable device powered by magnetic resonant coupling allows for optogenetic stimulation of regions of the deep brain, with reliable operation and good chronic stability via an ultrathin injectable probe with a μ-ILED at its tip[123] (Fig. 2e). The small footprint (diameter of ~9.8 mm), thickness (<1.3 mm after encapsulation) and lightweight construction (~30 mg) of the device, along with its mechanical flexibility, allow for stable output power when bending to radii of curvatures less than 5 mm. A double-loop primary coil supports simultaneous operation of a large collection of devices in all regions of a standard home cage (30 × 30 cm) with good spatial uniformity (variation of light intensity on the same height was less than 30%). A bilayer encapsulation of parylene and PDMS ensures good biocompatibility and long-term stability. The devices can operate continuously in complex environments that contain obstructions and metal surroundings, including water tanks.

The power-transfer efficiency of magnetic resonant coupling is determined by the coupling coefficient, κ, between the primary and secondary coils, as well as by their Q-factors[165]. Both κ and Q-factor decrease with the coil size, leading to significantly reduced power-transfer efficiency for devices with size <10 mm^2. Also, κ rapidly decreases with the distance (and lateral misalignment) between primary and secondary coils[165,181]. Ultraminiaturized implants[146] therefore require optimized magnetic coupling schemes and coil designs; this requirement can be mitigated for small animals by employing primary coils that enclose the test arena[100]. Similar schemes for experiments in large animals are less practical, as high levels of input power are needed to maintain useful magnetic energy densities across areas of interest. An additional consideration is in reducing the resistance of the conductive traces to achieve coils with high Q-factors. Optimization requires a balance between trace thicknesses, overall dimensions and bending stiffnesses[98,102]. Despite these challenges, near-field magnetic resonant coupling represents the most widely adopted technology for operating wireless and battery-free implants in small animals, as shown with devices for physiological recording[143], optogenetic stimulation[102] and pharmacological modulation[144].

Photonic power transfer. Electromagnetic radiation in the form of visible and near-infrared light can also be exploited for wireless power delivery[123,124,142,158]. For example, dual-junction gallium arsenide (GaAs) solar cells with conversion efficiencies of 25% can support the operation of control logic circuits and of injectable μ-ILEDs for optogenetic stimulation. Compared with systems powered only by RF radiation, the addition of these solar cells, for a 1-sun light source, can reduce the amount of required RF power by at least tenfold[158]. Arrays of 3 × 5 microscale GaAs solar cells (built on

multilayer GaAs wafers using standard microfabrication techniques and transfer-printed onto flexible substrates) can drive blue and yellow μ-ILEDs at intensities of 3.5 and 2.3 mW mm^{-2} (~19 mW cm^{-2} with an array area of 6 × 2 mm) under infrared illumination (774 nm; with an intensity of 200 mW cm^{-2}), and can power wireless optogenetic devices[142].

Recent developments in the monolithic integration of microscale optoelectronic devices serve as a practical basis for power harvesting in ultraminiaturized wireless implants[123,124]. For example, a thin-film upconversion device that combines an infrared double-junction photodetector and a visible LED, both based on III–V semiconductor optoelectronic technologies[124], captures photons (810 nm) from an external source and generates a photovoltaic current (with a power density of ~2.1–9.5 mW cm^{-2}) that in turn powers the LED to realize visible-light emission (590–630 nm in wavelength) for optogenetic stimulation (Fig. 2g). A miniaturized wireless optoelectronic neural interface (microscale optoelectronically transduced electrodes) includes 180-nm complementary metal–oxide–semiconductor (CMOS) circuits to amplify and encode neural signals with an AlGaAs photodiode that switches between photovoltaic modes for power harvesting (with a power density of ~12 mW cm^{-2} on a diode area of ~50 × 80 μm) and LED modes for data communication (near-infrared emission) with external systems[123]. This ASIC device enables the development of small implants (4.7×10^{-3} mm^3) with low power consumption (1 μW) as potential foundations for electrophysiological recording or stimulation at high spatial resolution and at specific discrete sites within single neurons or single muscle fibres.

An analysis of total power requirements for these approaches, assuming uniform illumination of an experimental arena, is instructive. For example, in the case of the double-junction photodetector upconversion device, the infrared light intensity required to generate useful optical emission is 15 mW mm^{-2}, which corresponds to a power of 562.5 W for a home cage of 15 × 25 cm (ref. [124]). Similarly, an infrared intensity of 200 mW cm^{-2} for the microscale GaAs solar-cell array corresponds to a total power of 75 W (ref. [142]). The green light used to power the microscale optoelectronically transduced electrodes is 100 mW mm^{-2}, which is equivalent to 3,750 W (ref. [123]). Assuming infrared LED efficiencies of ~40% and considering power losses due to absorption or scattering by the scalp, skull and brain tissues[182], this leads to power levels that mandate either small experimental arenas or optical imaging or tracking systems, potentially combined with focusing optics, that may impose constraints on uses with freely behaving animals. The output power of solar cells strongly depends on incident angles[183], which may limit device operation in complex experimental arenas.

Ultrasonic power transfer. In this scheme, ultrasound waves emitted by a transducer can be converted to electrical power by a piezoelectric crystal[140,184,185]. Such waves propagate with a velocity 10^5 times slower than electromagnetic waves, and therefore have much shorter wavelengths (0.3–0.7 mm for ultrasound used in medical imaging) at similar frequencies. Hence, focused power delivery to implantable medical devices can be achieved with high spatial resolution[186]. For example, a miniaturized implantable ultrasonic backscattering sensor composed of a piezocrystal, a transistor and a pair of electrodes can support the wireless recording of electromyogram (EMG) and electroneurogram (ENG) data[126] (Fig. 2f). A disadvantage of this approach is that ultrasonic waves propagate directionally. As a result, slight misalignments and misorientations between the external transducer and the implanted receiver lead to reductions in coupling efficiency. Additionally, the transducer must contact the skin to eliminate a large impedance mismatch at the tissue–air interface. The large size of commercially available transducers hinders their practical use in awake and freely behaving small animals. A possible solution to misalignment challenges exploits beam-steering strategies enabled by miniaturized and wearable transducer arrays operated using sophisticated control algorithms[187]. Another difficulty is that high-performance inorganic piezoelectric crystals have brittle mechanical properties, comparatively high mass densities and rigid and planar characteristics that may limit their applications in small animals, for which high power output and mechanical compliance are important. For example, assuming a typical acoustic-to-electrical conversion efficiency of 2% (ref. [181]; maximum efficiency of ~25% for a perfect alignment between the transducer and the receiver[126]) and an implant cross-section of ~1 mm^2, the generation of milliwatts of power at the implant would require ultrasound intensities at the limit of exposure (7.2 mW mm^{-2}) approved by the US Food and Drug Administration[188]. To generate sufficient power (>10 mW) for applications such as those in optogenetics with ultrasonic power densities within the safety limit, the piezocrystal must present a large area, which implies the use of piezocrystals weighing hundreds of milligrams (in the case of lead zirconate titanate (PZT)). With standard transducer output intensities, the required area of the transducer and the battery-storage capacities for this scenario may pose practical difficulties in experiments with small animals.

The fundamental limit for ultrasonic power delivery is set by the ultrasonic attenuation that follows from the scattering and absorption of ultrasound waves. This quantity is proportional to $2\alpha f$, where α (dB cm^{-1} MHz^{-1}) is the attenuation coefficient and f (MHz) is the ultrasonic frequency[189]. Values of α for soft tissue, bone tissue and lung are ~0.4, ~20 and ~40, respectively[190]. Therefore, the ultrasonic attenuation calculated using reported ultrasonic frequencies[125,126,186] are ~0.8–1.48 dB cm^{-1}, ~40–60 dB cm^{-1} and ~80–120 dB cm^{-1} for soft tissues, bones and lung, respectively (Table 1). The relatively moderate absorption of ultrasound by soft tissues potentially enables large penetration depths[181], but the presence of highly absorbing bone may induce significant heating effects[191], and low ultrasonic frequencies may induce cavitation[189].

Overall, recent efforts show that the size and mechanical loads associated with conventional electrochemical power sources can be greatly reduced by using instead wireless and lightweight systems with capabilities in power supply that support advanced neuromodulation and sensing capabilities for use in small animals. This new generation of tools creates many new opportunities for basic studies of the peripheral and central nervous systems in freely moving animal models, and forms the technological basis for potential translation to large animal models, non-human primates and human applications.

Operation modes. Operation modes can be addressed via power-delivery schemes and device configurations selected for different anatomical locations, recording requirements and stimulation capabilities. For instance, subdermal implantation for the neuromodulation of mouse brains is only possible with devices that are small (<1 cm^2) and lightweight (<0.5 g). Simple stimulation can be realized by passive components, whereby changes in the frequency and duty cycle of the power transmitter control the temporal pattern and strength of stimulation. Examples include devices powered by RF transmission[98,122] or magnetic coupling[192] for stimulation of the deep brain[100,122], spinal cord[122,192] and peripheral nerves[98,122]. Systems with independently addressable biointerfaces that stimulate distinct anatomical locations at the cellular[193] and circuit level[194] require multichannel wireless operations that can be addressed by passive multiresonance antennas. Active components can support the digital control of individual and multiple devices[102], thereby eliminating issues of spatial- and orientation-dependent RF coupling. Predefined program states

stored in the non-volatile memories of low-power microcontrollers can control the magnitude and spatial and temporal patterns of multiple stimulators in individual or multiple devices[102]. The monolithic integration of multifunctional neuromodulation devices can feature combinations of soft microfluidic channels and μ-ILED probes for programmable and coordinated delivery of pharmacological and optogenetic stimuli, configured as injectable probes for insertion into regions of the deep brain[62] and as soft cuffs for wrapping peripheral nerves[144].

For wireless and fully implantable devices that involve physiological recording capabilities, uplink communication systems send data to external receivers for storage and further processing[195]. Solutions using protocols based on Bluetooth radios, NFC, ultrawideband, infrared communication and ultrasonic backscattering each have distinctive advantages and disadvantages in terms of data rate, operation distance and the inherent compromise in form factors and power consumption[196].

Infrared LEDs for optical communication enable device sizes that are less than 1 × 0.5 mm and with power consumptions lower than 0.5 mW (ref. [131]) for sampling rates at ~27 Hz with 12-bit resolution, which are sufficient for capturing temporal variations in regional oxygen saturation levels associated with tissue perfusion, in global oxygen levels (below 1 Hz)[143] and in neuronal calcium dynamics[60,131]. An optical link can also be used for both power supply and data transmission in ASIC-enabled electrophysiological recording devices with submillimetre form factors and with potential for fully implantable operation[123].

Systems that integrate neural recording with neuromodulation in open-loop or closed-loop modes have additional requirements for bidirectional communication[61,107,145,195,197], such as downlinked control commands and uplinked recorded signals via either the same or a separate mechanism[195]. Closed-loop feedback involves the real-time adjustment of the timing and amplitude of modulation (stimulation or inhibition) in response to neural activity or physiological responses, and is clearly advantageous over open-loop systems, particularly for therapeutic purposes[107,198]. There are substantial engineering challenges to retaining the key features needed for operation in this mode with implantable systems that allow unconstrained animal experiments. An example of a wireless closed-loop system involves the regulation of bladder function in a rat via the combination of magnetic resonant coupling for power supply and Bluetooth low-energy protocols for bidirectional data transmission[141]. The system records biophysical signals related to bladder filling and voiding and transmits them to an external device, via a wireless Bluetooth Low Energy communication protocol, automatically identifying bladder dysfunction, thus controlling the activation of μ-ILEDs for the optogenetic regulation of voiding events.

ASICs designed for implantable wireless devices for physiological recording and neuromodulation can vastly improve the characteristics of systems that rely on discrete off-the-shelf components by facilitating ultralow power requirements (down to the nanowatt level[129]), exceptionally small form factors (down to the submillimetre level[123,146]) and high integration densities (over 100 channels[61,199]). The performance gains in ASICs follow from specialized circuit designs that omit flexible and programmable control structures; however, this customization limits their versatility. Also, each application requires a cycle of design, development and production, as a lengthy and costly process that further delays refinements and modifications. As a result, ASICs have limited appeal for exploratory research carried out by individual investigators or small university teams because, in many cases, the requirements and functionalities are often not clearly defined. Hence, in spite of numerous research demonstrations, only a few ASICs (such as Intan microsystem chips for multiplexed recording and stimulation, and Neuropixel probes for the deep brain with integrated amplification) have been deployed and adopted for neuroscience research. By contrast, off-the-shelf components offer significantly more flexibility and cost effectiveness, for rapid implant design and verification in a scalable format.

Optogenetic stimulation

Microscale optoelectronic components enable highly miniaturized devices for in vivo optogenetics, such as μ-ILEDs with lateral sizes as small as 10 × 15 μm² and thicknesses of 0.5 μm (ref. [53]) with a wide range of options in emission wavelengths (ultraviolet, blue, green, yellow and red) and optical output intensities (50 mW mm^{-2} and more[53,100]) that are suitable for most optogenetic experiments (using, for example, 1–21 mW mm^{-2} to activate channelrhodopsin[45,98,122,200–202], the red-shifted variants of channelrhodopsin C1V1 (ref. [202]) and ReaCHR[203], and halorhodopsin[204]). In pulsed-mode operation, the maximum steady-state temperatures at the interface with the tissue are less than a few tenths of a degree Celsius[102], which is well below the safety thresholds (2–5 °C) for irreversible tissue damage[205,206], the 2 °C limit for neurostimulators[207] and the approximate 1 °C limit for thermal neuromodulation[208]. Such μ-ILEDs have electrical operating requirements that can be satisfied by a range of wireless power sources. For example, fundamental studies indicate levels of irradiation suitable for stimulating single neuronal units (0.1–0.2 mW mm^{-2}) and for activating groups of channelrhodopsin-expressing neurons (1 mW mm^{-2}) at the surface (150 μm²) of an InGaN μ-ILED operated with ~10 μW (~2.9 V and ~3 μA) of electrical power for single-unit operation and with ~25 μW (~3.1 V and ~8 μA) for multiunit operation[53]. Additional optical power can yield volumetric illumination to evoke strong behavioural effects. The typical electrical power associated with μ-ILEDs for optogenetic stimulation in freely behaving animals is 1–3 mW. This power, which yields light intensities of ~10 mW mm^{-2} (refs. [98–100]), is within the range accessible to most wireless schemes.

Representative miniaturized optogenetic systems interfaced with such μ-ILEDs use schemes of wireless control and power supply based on lightweight (~700 mg) power harvesters (910 MHz, far-field RF transmission and panel antenna) with sets of gallium nitride μ-ILEDs (50 × 50 × 6.5 μm³) on thin (6 μm thick) polyester probes[99] (Fig. 3a). This design architecture also enables multimodal operation via the combined integration of μ-ILEDs, photodetectors, temperature sensors and platinum electrodes for simultaneous optogenetic stimulation, thermal monitoring and electrophysiological recording at the same location in a targeted area of the deep brain. Mechanical compliance and flexibility of the probe (total thickness of 20 μm and width of 300 μm) reduces glial activation and lesion sizes (compared with those caused by optical-fibre probes). Optogenetic demonstrations in mice include place-preference and anxiety-like behaviour modulation[99].

Similar designs but with stretchable RF energy harvesters and μ-ILEDs in soft polymer matrices (particularly PDMS, with an effective modulus of 1.7 MPa) can yield mechanics and form factors that allow effective integration with soft biological tissues in highly mobile areas of the peripheral nervous system and the spinal cord[98] (Fig. 2d). Stretchability (strains up to 30%), miniaturized geometry (~16 mm³) and lightweight construction (~16 mg) enable robust operation for 6 months or more after subdermal implantation and reliable function under physiological strains in freely behaving animals[98]. Optimized designs (2.34 GHz and far-field RF transmission) can reduce the antenna areas (3 × 3 mm) by two orders of magnitude relative to those of conventional approaches based on battery power. The wide bandwidths (200 MHz) of such antennas further reduce the effects of slight mismatches between the central operating frequency of the antenna and the RF transmitter[98], allowing for functional place-aversion experiments with both the sciatic nerve and spinal cord of mice expressing a channelrhodopsin.

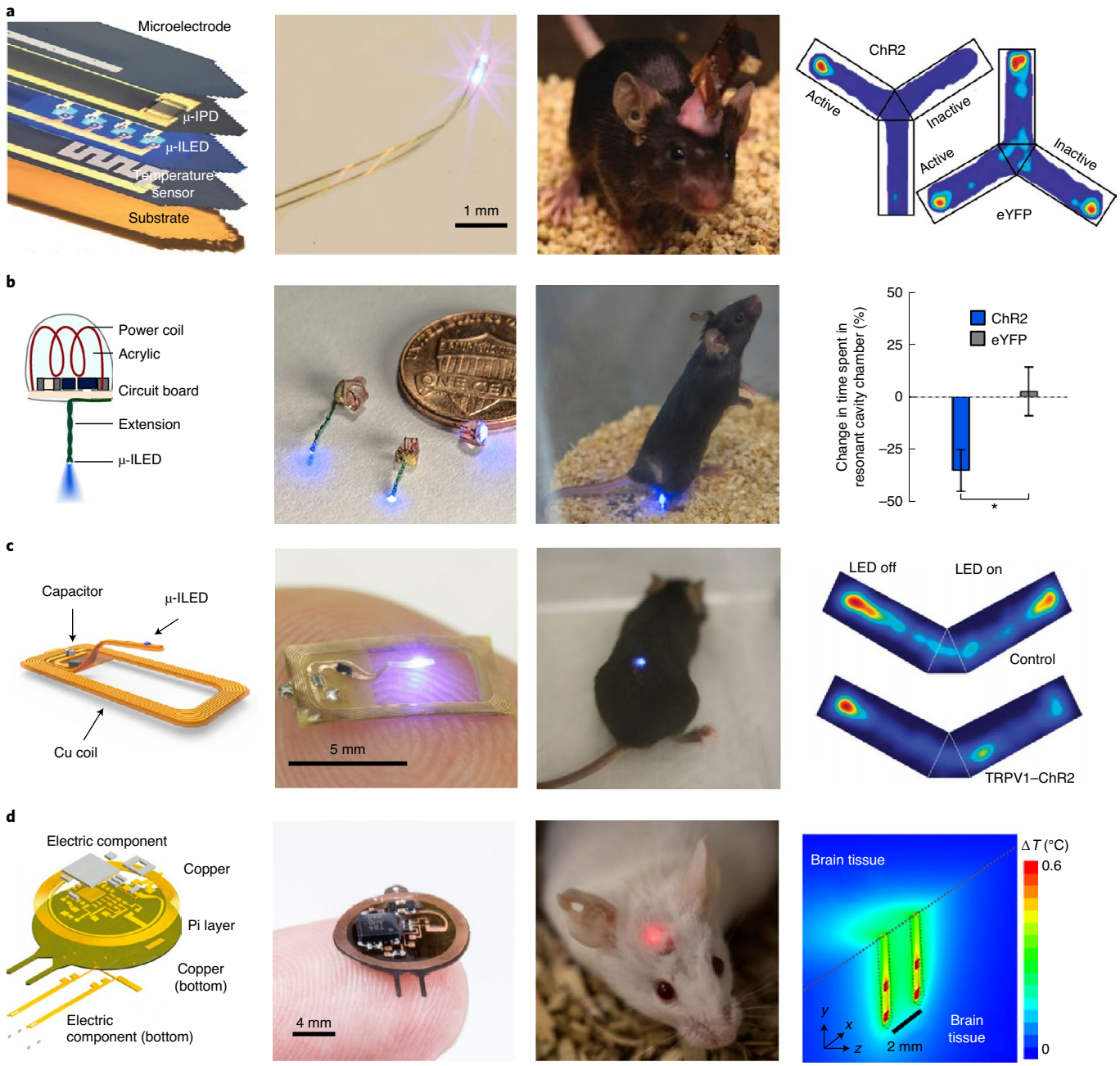

Fig. 3 | Optogenetic interfaces for the regulation of cell activity. a, An injectable probe for optogenetic stimulation, electrical recording, temperature sensing and photometry. μ-IPD, microscale inorganic photodetector; μ-ILED, microscale inorganic light-emitting diodes. **b**, Miniaturized implantable optogenetic probes, powered by a RF generator and a resonant cavity, for neuromodulation in the brain, spinal cord and PNS. **c**, An optogenetic probe in a thin and flexible open architecture, powered by near-field magnetic resonant coupling, for long-term use in the spinal cord. **d**, An implantable optoelectronic system, consisting of four μ-ILEDs on two bilateral probes and an integrated circuit, for stable multimodal interfaces during chronic operation. Pi, polyimide. Each panel includes a schematic, an optical image, the implantation of the device in the animal model, and a functional demonstration. Figure reproduced with permission from: **a**, ref. [99], AAAS; **b**, ref. [122], Springer Nature America, Inc.; **c**, ref. [192], Wolters Kluwer Health, Inc; **d**, ref. [102], Springer Nature Ltd.

Related embodiments support miniaturized systems (0–25 mm^3 and 20–50 mg) that exploit the RF resonant-cavity approach. The devices consist of hand-wound coils, μ-ILEDs and circuitry for application in the premotor cortex and spinal cord[122] (Fig. 3b). The cavity (21 cm in diameter and 15 cm in height) generates localized electromagnetic energy (1.5 GHz) selectively coupled into the bodies of mice at all positions within a custom experimental cage. Functional demonstrations have shown increased circling locomotion and reflexive nocifensive behaviour via optogenetic stimulation (blue light, 6–40 mW mm^{-2}) in the right premotor cortex and in the spinal cord of transgenic mice expressing, respectively, Thy1–ChR2–eYFP (the light-activated ion channel channelrhodopsin-2 (ChR2) fused to enhanced yellow fluorescent protein (eYFP) under the control of the promoter thymus cell antigen 1 (Thy1)) and the proto-oncogene c-Fos (ref. [122]).

Optoelectronic devices based on near-field magnetic resonant coupling at 13.56 MHz (Fig. 2e) exploit flexible printed-circuit-board technology (copper metal traces on the top and bottom of a polyimide substrate) for the antenna and injectable needle, and enable wireless power transmission and positioning of the μ-ILEDs into

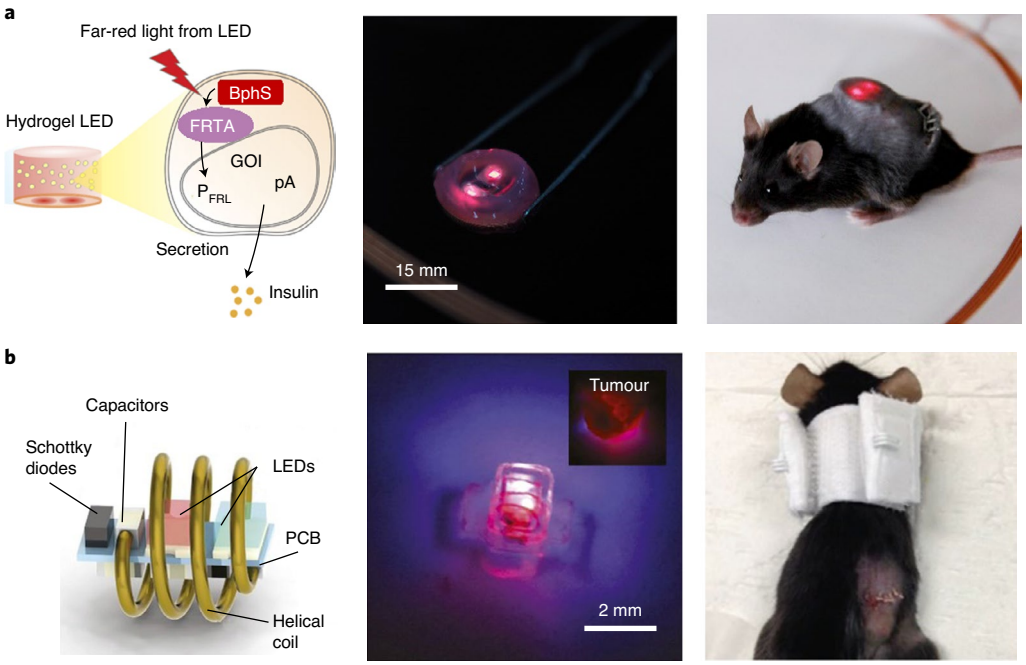

Fig. 4 | Implantable and wireless devices for photonic therapy. a, An optogenetic stimulation system for remotely controlling the release of glucose-lowering hormones from optically engineered cells in diabetic mice. BphS and FRTA, transcription regulators; GOI, genes of interest; pA, polyadenylation signals; P_{FRL}, vector containing luciferase genes. **b**, An optoelectronic device, wirelessly powered by RF radiation, for photodynamic therapy at the target site, where the system modulates light emission for optimum therapeutic dosage. PCB, printed circuit board. Figure reproduced with permission from: **a**, left, ref. [216], AAAS; **b**, ref. [217] National Academy of Sciences.

the deep brain as well as optogenetic studies of the spinal cord (Fig. 3c) and of various parts of the peripheral nervous system[100,192,209]. Miniaturized geometries (10 mm^3) and lightweight (~20 mg) construction also enable complete subdermal implantation without altering locomotor function or inducing anxiety-like behaviour, as determined by comparisons to sham-operated controls[192]. The designs allow for mechanical flexing with minimal changes in power-transmission efficiency (change of *Q*-factor of <0.12) or resonance frequency (<0.1 MHz), even for bending to radii of curvatures of 5 mm, for reliable operation under natural movements. Experimental demonstrations include optical activation of TRPV1–ChR2 (a transient receptor potential vanilloid-1 receptor and channelrhodopsin-2) in spinal afferents, which results in real-time place aversion in freely behaving mice[192].

The coordinated dissection of neuronal populations at multiple locations and the selective modulation of individual subjects in social behavioural studies requires precise control over the intensity of the stimulation and over multiple devices and multiple light emitters in a single device. These capabilities can be supported by active electronic designs with programmable simplex communication schemes enabled by binary on–off-keying protocols for sending commands to the implant[102] (Fig. 3d). The patterns of optical stimuli are achieved by a microcontroller that provides timing and illumination information for activating the μ-ILEDs. As an example, the independent operation of multiple μ-ILEDs on separate probes and four μ-ILEDs for bilateral operation (Fig. 3d) allow optogenetic neuromodulation of spatially distinct sites with programmable frequencies and duty cycles[102]. In separate embodiments, programmable and precise control over emission intensity, realized by an additional digital-to-analog circuit that provides output frequencies as high as 1.5 kHz, can be used for rapid, in vivo characterization of new opsins and for interrogation of neural circuits with high temporal resolution. Active power management can be achieved with a low-dropout linear regulator coupled with a pair of time-multiplexed antennas to yield power-harvesting performance that is invariant to position and angular orientation and a stable direct-current power supply for the circuits and μ-ILEDs. These advanced modes of operation are possible without significantly increasing device size or weight, thereby retaining all of the attractive features associated with the form factors of the corresponding passive systems. An additional feature of this device type is the absence of magnetic components, which renders compatibility with magnetic resonance imaging on implanted animals. The results provide insights into the location of the implants as well as into the status of surrounding tissues in vivo.

Photonic therapy

The potential of optogenetics for therapeutic applications is indicated by experimental demonstrations in the restoration of visual function in animals with retinitis pigmentosa[210–212], the control of spontaneous epileptic seizures[213,214] and the regulation of cardiac pacing and resynchronization activity[215]. In another example, a set of wirelessly powered LEDs (far-red light, 730 nm) implanted in mice with diabetes can activate photoreceptors (monophosphate synthase) that initiated insulin gene expression[216] (Fig. 4a). In this system, customized transmitting coils around the cage provide electromagnetic power (magnetic resonant coupling at 180 kHz) to the implant. The experiments use wireless delivery of insulin for rapid restoration of homeostatic blood glucose in freely moving animals. A user interface paired with a separate Bluetooth-enabled glucose monitor further enable the semiautomatic glycaemia-dependent activation of a wireless power transmitter that controls the brightness of the LED and the illumination time.

Other means to exploit light–tissue interactions include photodynamic therapy, whereby light activates certain types of drug or photosensitizer to deliver pharmacological agents to targeted areas in a controlled manner. For example, miniaturized (15 mm^3, 30 mg)

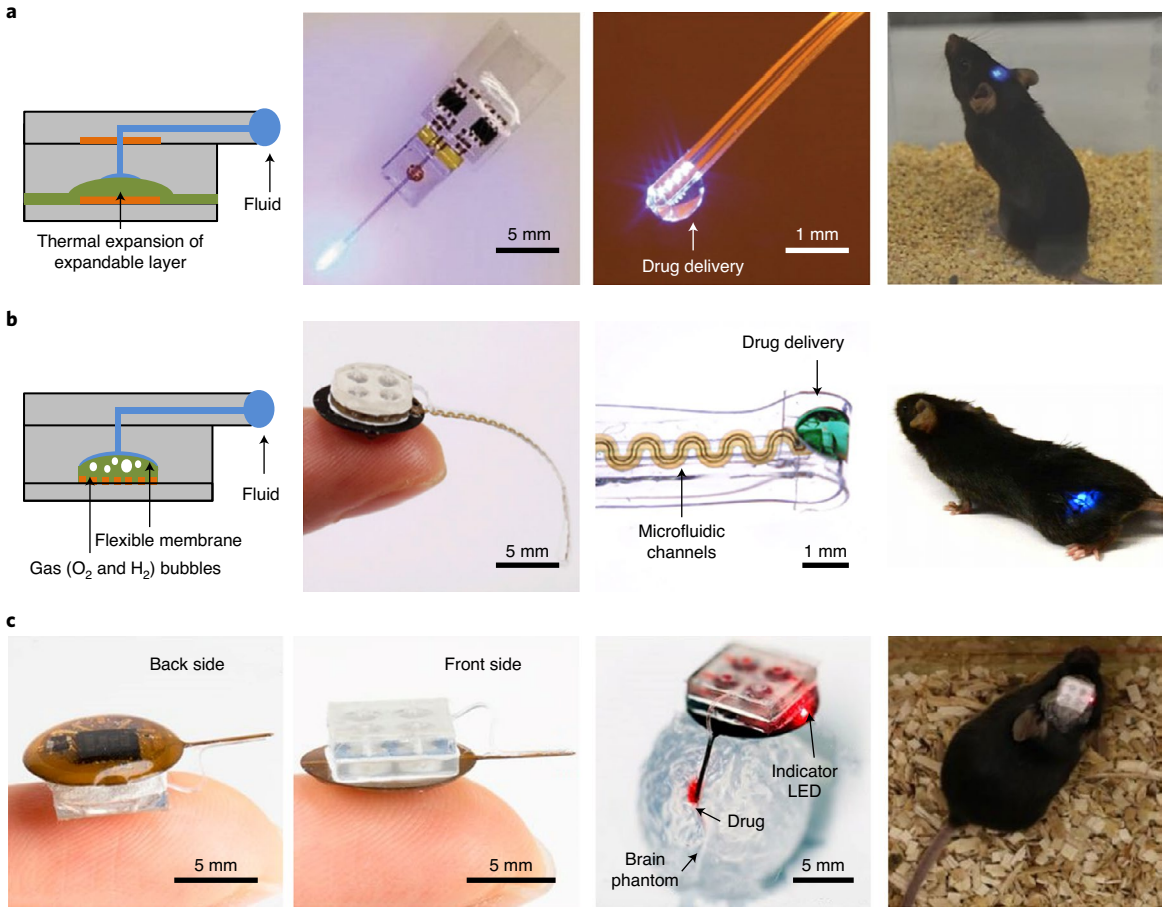

Fig. 5 | Wireless systems for the programmed microfluidic delivery of pharmacological agents. a, An optofluidic probe and thermally actuated pump that integrates Joule-heating elements with thermally expandable materials (as mechanical actuators to pump fluid), and with a RF-powered wireless module and microcontroller for independent fluid delivery from four separate chambers to regions of the deep brain. **b**, An optofluidic cuff system and electrochemical pump for the programmed delivery of light and pharmacological agents to peripheral nerves. **c**, Injectable microsystems for programmable optogenetics and pharmacology at targeted areas of the deep brain. Figure reproduced with permission from: **a**, ref. [226], Wiley; **b**, ref. [144], AAAS; **c**, ref. [62], National Academy of Sciences.

optoelectronic devices wirelessly powered with RF radiation (frequencies of 1–1.5 GHz) can activate photosensitizers (chlorin e6) through thick (>3 cm) tissues for suppressing tumour growth in mouse models of cancer[217] (Fig. 4b). The device in this case consists of a three-turn coil for wireless power harvesting and a rectifier that converts RF into a direct current to drive two LEDs (red, 660 nm, and violet, 400 nm) encapsulated in PDMS. This device focuses on light-actuated therapy to induce apoptosis in tumour cells; however, the foundational materials and engineering approaches can be adapted for other types of neural interface system.

Microfluidic delivery of drugs

Devices with capabilities in pharmacological delivery provide unique opportunities for cell-specific and tissue-specific targeting. For example, optogenetic and chemogenetic systems can be combined for light-dependent activation of a pharmacological agent[19,218–223] and for deep-brain stimulation for psychiatric disorders[224]. Conventional drug-delivery systems rely on syringe injection or on metal cannulas coupled to reservoirs and micropumps via tubing. The disadvantages are similar to those of other types of tethered systems, although even more considerable owing to the thick and stiff tubing needed for efficient fluid transport. Wireless powering and control strategies for compact microfluidic systems that incorporate reservoirs, valves, pumps and channels for the delivery of multiple pharmacological agents to highly localized target locations (such as the deep brain or the spinal cord) are therefore advantageous. Recently reported systems incorporate soft microfluidic probes in multilayer architectures to support multimodal operation, with options for optical, electrical and chemical sensing and activation. Integrated pumps eliminate the need for external fluid-handling hardware or syringe pumps[225]. One example uses μ-ILEDs integrated with microfluidic probes (500 μm × 8 mm × 80 μm), compact thermally actuated pumps and associated reservoirs (~73 mm^3), along with a dual-channel RF control module (~52 mm^3; peak power transmission at 1.8 GHz and 2.9 GHz) as part of a miniaturized (~125 mm^3), lightweight (220 mg) and flexible system[226] (Fig. 5a). The fluid reservoir and pump exploit a thermally expandable composite material for 90% delivery efficiency (~0.46 μl from a 0.5-μl reservoir) via the activation of an associated Joule-heating element (~100 °C). The reservoir consists of a cyclic olefin polymer, which has a low water-vapour permeability (0.023 g mm m^{-2} d^{-2}). This system allows operation in freely behaving animals with little impact on behaviour. Disadvantages are mainly in the high power consumption of the thermal-mechanical pumping mechanism and the absence of a means to refill the reservoir for multiple cycles of use.

Recent work addresses these limitations through the use of magnetic resonant coupling for power transfer and of electrochemical pumps for power-efficient operation[144] (Fig. 5b). In a version

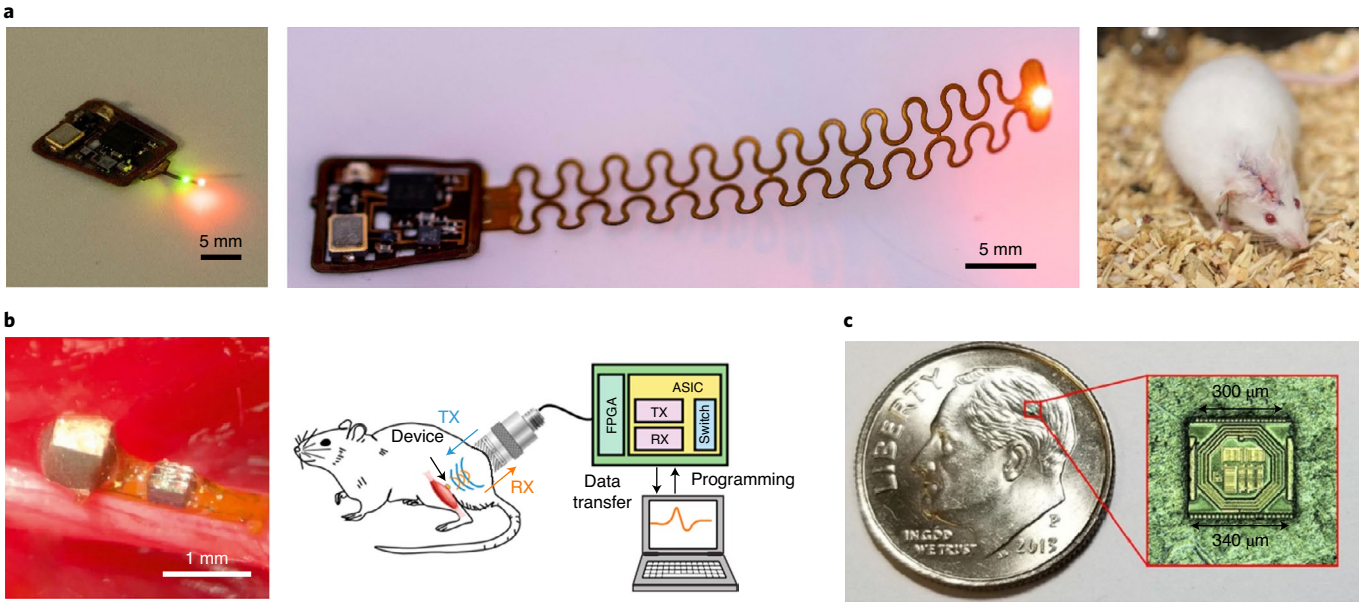

Fig. 6 | Wireless systems for biosignal recording. a, A wireless optoelectronic system for the continuous monitoring of localized tissue oxygenation at sites of interest, such as peripheral tissues and the deep brain. **b**, An ultrasound-based device for measuring EMGs and ENGs from the gastrocnemius muscle and sciatic nerve, respectively. FPGA, field-programmable gate array; RX, signal reception; TX, signal transmission. **c**, A miniaturized neural interface based on a 130-nm CMOS fabrication process for the neural recording and bipolar stimulation of the sciatic nerve. Figure reproduced with permission from: **a**, ref. [143], AAAS; **b**, ref. [126], Cell Press; **c**, ref. [146], IEEE.

designed for interfaces to peripheral nerves, the device consists of (1) a low-modulus (~3 MPa) elastomeric cuff that surrounds a targeted nerve, (2) four microfluidic channels (total thickness of 200 μm and a cross-sectional area of $60 \times 60\ \mu m^2$) along the length of the probe that leads to the cuff, and (3) a μ-ILED integrated on the cuff for light delivery. The section of the implant responsible for wireless energy harvesting, electronic control and pumping (radius of 5 mm and thickness of ~4 mm) also stores the drugs in sealed reservoirs. Four electrochemical pumps (~1.5 μl) consume low power (~800 μW) in the electrolysis of water to produce pressure via the generation of oxygen and hydrogen gas (used to generate the driving force to pump the drugs) with high levels of control. The fully assembled system weighs only 0.3 g (compared with 1.8 g for the thermally actuated system with an assembled battery[16]), with minimal impact on the animal. Experimental demonstrations in freely behaving animals with the optical activation (blue, 470 nm) of excitatory neurons expressing channelrhodopsin-2 resulted in place aversion in a Y-maze experiment where only one arm of the experimental enclosure involved optogenetic stimulation. Conversely, a reduction in pain threshold, specifically in thermal sensitivity, was achieved with the local delivery of the anaesthetic bupivacaine ($40\ mg\ ml^{-1}$). The soft mechanics of the cuff (made of PDMS) led to minimal irritation of the nerve (compared with otherwise similar structures made from poly(ethylene)).

Modification of this same system using μ-ILEDs and an injectable needle as support for thin and soft microfluidic channels ($0.35 \times 0.1\ mm^2$ and a modulus of 3 MPa) allow for use in targeted areas of the deep brain[62] (Fig. 5c). Surgical insertion of such a probe into the brain and fixation of the device (0.3 g) on top of the skull did not disrupt normal locomotion. Notably, the use of such lighter and less obtrusive systems shows substantially higher baseline locomotion compared with battery-operated devices (1.86 g). The high degree of mechanical compliance of the probe further reduces lesioning ($0.068\ mm^2$ compared with $0.184\ mm^2$ via a metal cannula with a diameter of 0.46 mm)[62] and immunoreactive glial responses (compared with those associated with conventional cannulas). In a demonstration experiment using this brain-interfaced optofluidic device, optical stimulation of the ventral tegmental area of wild-type mice increased locomotion behaviour, whereas concurrent wireless infusion of a *N*-methyl-D-aspartate receptor antagonist blocked this activity. The use of multiple independently addressable reservoirs enables multiple infusion events; for instance, the infusion of viruses or tracers in combination with optogenetic stimulation could provide additional information on neuronal circuit dynamics.

Biosignal recording

Most technologies for wireless optogenetics and pharmacology focus on manipulating neuronal or cellular activity rather than on recording or sensing. For the precise interpretation of behaviour of the central and peripheral nervous systems, capturing neural and other physiological activities with high fidelity is crucial. Recent advances in electronics and microfabrication techniques enable recording with on-board signal processing that involves filtering, amplification and digitization.

For example, progress in the miniaturization of battery-free electronics and data communication systems serves as the basis for fully implantable wireless platforms that can measure the oxygen saturation of targeted tissue (such as the deep brain) in freely behaving animals[143] (Fig. 6a). Key components in the small device (lateral dimensions of $10 \times 10\ mm^2$, thickness of ~0.25 mm and weight of 0.1 g) reported in ref. [143] include microscale optoelectronic elements (μ-ILEDs and a microscale inorganic photodetector) for recording of local haemoglobin dynamics, and subsystems for continuous wireless delivery of power and for data transfer. Radiometric measurements that leverage differences in the absorption of haemoglobin in its oxygenated and deoxygenated states revealed the oxygenation dynamics of the target tissue. The device can resolve oxygen saturation levels in small tissue volumes defined by the illumination profiles ($0.5–2\ mm^3$). Such measurements can yield insights into the underlying mechanisms of regional oxygen-mediated biological processes (such as neural activity, tissue perfusion and wound healing)[227–229], and can be used to

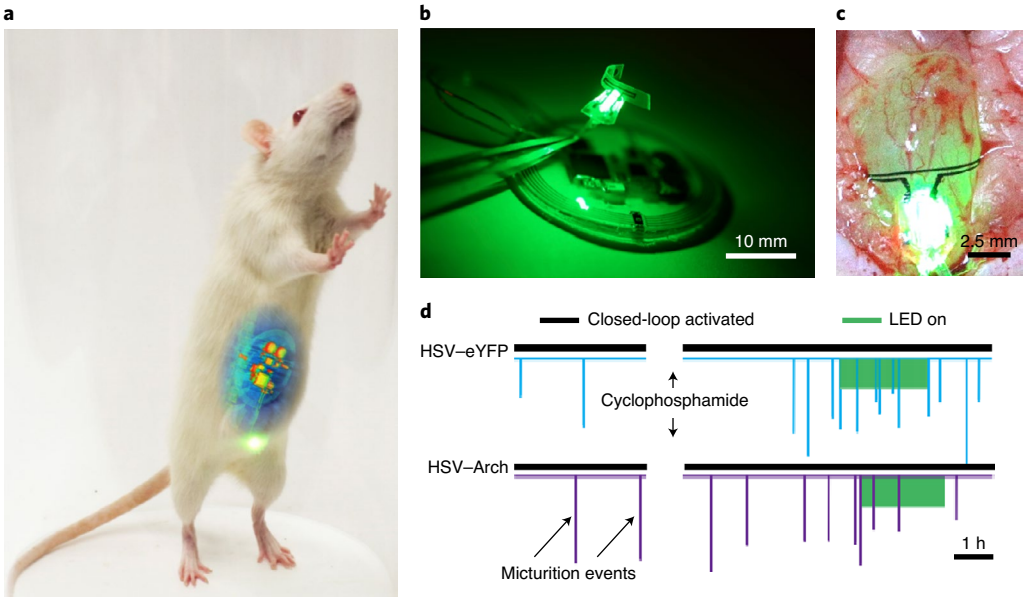

Fig. 7 | Fully implantable, wireless and battery-free system for automated closed-loop peripheral neuromodulation. a, A rat with an implanted device during activation of the μ-ILEDs. **b**, A device that combines a wireless control-and-power management module, an optical sensing-and-stimulation module and a wireless power-transfer module. **c**, Optical image of a strain gauge and μ-ILEDs wrapped around the bladder of a rat in an expanded state. **d**, Closed-loop optogenetic neuromodulation showing that rats injected with HSV-Arch-eYFP (a combination of herpes-simplex viral vector, opsin archaerhodopsin 3.0 and eYFP) experienced fewer voiding events after the injection of cyclophosphamide to induce voiding dysfunction than control rats injected with HSV-eYFP. Panels **c** and **d** reproduced with permission from ref. [141], Springer Nature Ltd.

provide therapeutic guidance, to inform real-time organ health and to aid in closed-loop regulation of physiological processes.

Another example involves ultrasound sensors attached to a peripheral nerve and to skeletal muscle that measure both ENG and EMG signals[126,230] (Fig. 6b). The device (2.4 mm^3) consists of a piezocrystal (~0.42 mm^3), a custom integrated circuit (0.5 × 0.45 mm^2) and gold recording electrodes (0.2 × 0.2 mm^2), packaged within medical-grade ultraviolet-curable epoxy. Data communication relies on the modulation of backscattered waves, which carry analog information from the EMG and ENG signals. Initial demonstrations illustrate the recovery of ground-truth action potentials (with ~90% correlation). A recent example used related methods in a further miniaturized neural recording implant (0.8 mm^3) placed in the motor cortex of an awake behaving rat[231,232].

The combination of mature silicon CMOS technologies and emerging wireless power-transfer schemes provides alternative strategies for ultraminiaturized devices that can both record and stimulate. For example, an ASIC system based on a 130-nm CMOS process includes the recording electrodes and a pair of composite electrodes integrated on the side walls of the CMOS die (both types of electrode were made of a mixture of conductive polymer and carbon nanotubes), an on-chip coil antenna for wireless power harvesting via magnetic coupling and CMOS circuits for operation control, all integrated on a single die with dimensions of 300 × 300 × 80 μm (Fig. 6c). Devices of this type enable direct injection into target areas via a syringe needle[146] (with an inner diameter of 0.4 mm) for distributed free-floating operations at multiple locations. The communication method provides sufficient bandwidth to address up to ten different devices via a frequency-division multiple-access system (0.5–3 GHz, with 250-MHz spacing). When implanted in the sciatic nerve of a rat, the device can deliver electrical stimulation and elicit action potentials in the axons, as evidenced by the EMG response.

The wireless systems highlighted here are aimed mainly at long-term biointegration. An emerging class of technology that focuses on transient applications, such as those in post-surgery monitoring, requires only limited operation times, and hence benefit from device dissolution or disintegration into benign end-products after a controlled period of stable operation within the body[233,234]. Such types of biodegradable systems have the potential to monitor[106,235] and treat[236,237] a variety of conditions without the need for surgical extraction procedures. For instance, entirely biodegradable and biocompatible electrical peripheral-nerve stimulators with wirelessly operated energy-harvesting systems (magnetic resonant coupling at ~5 MHz) and stimulating electrodes can yield accelerated functional recovery and neuroregeneration in injured peripheral nerves in rodent models[236].

Closed-loop operation

Conditional (or closed-loop) operations combine sensing and actuating capabilities, with real-time signal processing and modulation for identifying and controlling neural disorders[213] and for bridging dysconnectivity in injured neural circuits[36,238]. A single implantable device can be programmed to deliver stimulation when certain conditions are met (such as seizure onset)[141,239], and multiple devices (for stimulation and recording, for instance) can support closed-loop operation through a wireless link[216,240]. References [241,242] provide information on such conditions and the basic components.

A fully implantable, wireless and battery-free optoelectronic system with a conformal optogenetic interface for the stimulation of a peripheral nerve provides an example. Here, a soft biophysical precision sensor supports continuous measurement of organ function, with a wireless control-and-power module and a data analytics routine for the coordinated closed-loop correction of pathological physiology in real time (Fig. 7). The result enables automated neuromodulation with long-term stability (over 1 month) and minimally invasive operation[141]. In particular, the cell-specific stimulation of sensory afferent nerves innervating the bladder was achieved via the continuous monitoring of bladder function with an ultrasoft and stretchable strain gauge (~80 μm in thickness) as a

sensor of voiding, with associated real-time data analytics to identify overactivity. Automated optogenetic neuromodulation of bladder sensory afferents with μ-ILEDs (540 nm) on a platform collocated with the strain sensor enables the regulation of bladder function in the context of acute cystitis. The closed-loop operation involves real-time, multistep signal analysis (in particular, downsampling, smoothing and derivative calculation) to identify bladder voiding with >85% accuracy for a native bladder and with 95% accuracy for a cyclophosphamide-induced inflamed bladder. Device implantation in rats did not lead to significant immune responses, with no impairments in gait, movements or weight, or adverse effects on bladder cytometric properties over 7 days after implantation (compared with animals that underwent sham surgery). The data analytics and engineering approaches employed in this work, alongside the wireless control-and-power module and associated interface, can be adapted and combined with other functional systems, such as microfluidics and photometry, to yield systems for the regulation of the function of other organs.

Outlook

Wireless, battery-free implantable medical devices can now match, and in many cases exceed, the capabilities of many types of tethered system. These platforms integrate techniques and methods in soft materials, processing approaches, advanced wireless electronics, energy-harvesting schemes and microscale interface components. Highly miniaturized systems of this type can operate chronically in freely behaving small animals across nearly any part of the anatomy, and function as advanced diagnostic and therapeutic technologies in studies that require specific interfaces with various parts of the central and peripheral nervous systems. The ability to seamlessly monitor and regulate physiological processes without impact on the host animal yields capabilities that foreshadow powerful digital-health systems and engineered forms of therapies (such as electroceuticals or bioelectronic medicines) that leverage complementary research efforts in material-oriented approaches (for example, upconverting nanoparticles[1,24,25], magnetic nanoparticles[26–28] and ultrasound-based contrast agents[29,30]) within a multimodal system. Research and practical applications will rely on fundamental insights inferred from models of neuronal dynamics and connectivity, accurately established in untethered subjects. The technical maturity of the systems described in this Review Article have substantially evolved over the past 5 years, to the point that many are now commercially available as research tools. Others are in advanced stages of commercial development for use not only on animal models and cell assays but also in applications in human health.

Last, we highlight a number of important challenges and associated research opportunities. The first is in the realization of chronic in vivo operation with flexible devices, especially those that also have stretchable mechanics, where encapsulation schemes and designs at the biointerface must be ultimately configured to reach (and preferably exceed) human lifespans. The most significant hurdles in this context are those associated with complex systems that can provide advanced multimodal recording and stimulation capabilities via active electronics combined with soft materials in soft mechanical designs. The second is in improving the bandwidths in wireless communication schemes and in increasing the computational resources for the pre-processing of information on-device. A third challenge is in achieving reliable and efficient power supply, where unusual wireless power-transmission infrastructures may allow for device operation outside specialized environments. Finally enhanced sensing capabilities, particularly in technologies that can perform precise biochemical measurements, will add to the increasing volume of data and therefore to opportunities for the use of machine learning. These and other frontiers represent promising, multidisciplinary directions for research and development in neuroengineering.

Received: 21 March 2020; Accepted: 28 December 2020;
Published online: 8 March 2021

References

1. Rivnay, J., Wang, H., Fenno, L., Delsseroth, K. & Mallaras, G. G. Next-generation probes, particles, and proteins for neural interfacing. *Sci. Adv.* **3**, e1601649 (2017).
2. Hong, G. & Lieber, C. M. Novel electrode technologies for neural recordings. *Nat. Rev. Neurosci.* **20**, 330–345 (2019).
3. Jeong, J. W. et al. Soft materials in neuroengineering for hard problems in neuroscience. *Neuron* **86**, 175–186 (2015).
4. Tybrandt, K. et al. High-density stretchable electrode grids for chronic neural recording. *Adv. Mater.* **30**, e1706520 (2018).
5. Won, S. M. et al. Emerging modalities and implantable techonlogies for neuromodulation. *Cell* **181**, 115–135 (2020).
6. Azevedo, C. A. & Mammis, A. Neuromodulation therapies for alcohol addiction: a literature review. *Neuromodulation* **21**, 144–148 (2018).
7. Bouthour, W. et al. Biomarkers for closed-loop deep brain stimulation in Parkinson disease and beyond. *Nat. Rev. Neurol.* **15**, 343–352 (2019).
8. Fang, J. Y. & Tolleson, C. The role of deep brain stimulation in Parkinson's disease: an overview and update on new developments. *Neuropsychiatr. Dis. Treat.* **13**, 723–732 (2017).
9. Kuo, C. H., White-Dzuro, G. A. & Ko, A. L. Approaches to closed-loop deep brain stimulation for movement disorders. *Neurosurg. Focus* **45**, E2 (2018).
10. Wellman, S. M. et al. A materials roadmap to functional neural interface design. *Adv. Funct. Mater.* **28**, 1701269 (2018).
11. Robinson, J. T., Jorgolli, M. & Park, H. Nanowire electrodes for high-density stimulation and measurement of neural circuits. *Front. Neural Circuits* **7**, 38 (2013).
12. Fan, B. & Li, W. Miniaturized optogenetic neural implants: a review. *Lab Chip* **15**, 3838–3855 (2015).
13. Fu, R. et al. Implantable and biodegradable poly(L-lactic acid) fibers for optical neural interfaces. *Adv. Opt. Mater.* **6**, e1700941 (2018).
14. Gutruf, P. & Rogers, J. A. Implantable, wireless device platforms for neuroscience research. *Curr. Opin. Neurobiol.* **50**, 42–49 (2018).
15. Park, S., Loke, G., Fink, Y. & Anikeeva, P. Flexible fiber-based optoelectronics for neural interfaces. *Chem. Soc. Rev.* **48**, 1826–1852 (2019).
16. Jeong, J. W. et al. Wireless optofluidic systems for programmable in vivo pharmacology and optogenetics. *Cell* **162**, 662–674 (2015).
17. Pons-Faudoa, F. P., Ballerini, A., Sakamoto, J. & Grattoni, A. Advanced implantable drug delivery technologies: transforming the clinical landscape of therapeutics for chronic diseases. *Biomed. Microdevices* **21**, 47 (2019).
18. Sanjay, S. T. et al. Recent advances of controlled drug delivery using microfluidic platforms. *Adv. Drug Deliv. Rev.* **128**, 3–28 (2018).
19. Sim, J. Y., Haney, M. P., Park, S. I., McCall, J. G. & Jeong, J. W. Microfluidic neural probes: in vivo tools for advancing neuroscience. *Lab Chip* **17**, 1406–1435 (2017).
20. Liu, Y. et al. Soft and elastic hydrogel-based microelectronics for localized low-voltage neuromodulation. *Nat. Biomed. Eng.* **3**, 58–68 (2019).
21. Zhang, Y. et al. Climbing-inspired twining electrodes using shape memory for peripheral nerve stimulation and recording. *Sci. Adv.* **5**, eaaw1066 (2019).
22. Opie, N. L. et al. Focal stimulation of the sheep motor cortex with a chronically implanted minimally invasive electrode array mounted on an endovascular stent. *Nat. Biomed. Eng.* **2**, 907–914 (2018).
23. Yan, Z. et al. Three-dimensional mesostructures as high-temperature growth templates, electronic cellular scaffolds, and self-propelled microrobots. *Proc. Natl Acad. Sci. USA* **114**, E9455–E9464 (2017).
24. All, A. H. et al. Expanding the toolbox of upconversion nanoparticles for in vivo optogenetics and neuromodulation. *Adv. Mater.* **31**, e1803474 (2019).
25. Chen, S. et al. Near-infrared deep brain stimulation via upconversion nanoparticle-mediated optogenetics. *Science* **359**, 679–684 (2018).
26. Christiansen, M. G., Senko, A. W. & Anikeeva, P. Magnetic strategies for nervous system control. *Annu. Rev. Neurosci.* **42**, 271–293 (2019).
27. Roet, M. et al. Progress in neuromodulation of the brain: a role for magnetic nanoparticles? *Prog. Neurobiol.* **177**, 1–14 (2019).
28. Chen, R., Romero, G., Christiansen, M. G., Mohr, A. & Anikeeva, P. Wireless magnetothermal deep brain stimulation. *Science* **347**, 1477–1480 (2015).
29. Chu, P. C. et al. Neuromodulation accompanying focused ultrasound-induced blood–brain barrier opening. *Sci. Rep.* **5**, 15477 (2015).
30. Blackmore, J., Shrivastava, S., Sallet, J., Butler, C. R. & Cleveland, R. O. Ultrasound neuromodulation: a review of results, mechanisms and safety. *Ultrasound Med. Biol.* **45**, 1509–1536 (2019).
31. Farra, R. et al. First-in-human testing of a wirelessly controlled drug delivery microchip. *Sci. Transl Med.* **4**, 122ra121 (2012).

32. Abraham, W. T. et al. Wireless pulmonary artery haemodynamic monitoring in chronic heart failure: a randomised controlled trial. *Lancet* **377**, 658–666 (2011).
33. Stingl, K. et al. Artificial vision with wirelessly powered subretinal electronic implant alpha-IMS. *Proc. Biol. Sci.* **280**, 20130077 (2013).
34. Borton, D. A., Yin, M., Aceros, J. & Nurmikko, A. An implantable wireless neural interface for recording cortical circuit dynamics in moving primates. *J. Neural Eng.* **10**, 026010 (2013).
35. Finkelstein, A. et al. Three-dimensional head-direction coding in the bat brain. *Nature* **517**, 159–164 (2015).
36. Liu, X., Lu, Y., Iseri, E., Shi, Y. & Kuzum, D. A compact closed-loop optogenetics system based on artifact-free transparent graphene electrodes. *Front. Neurosci.* **12**, 132 (2018).
37. Martinez, D. et al. Adaptive quantization of local field potentials for wireless implants in freely moving animals: an open-source neural recording device. *J. Neural Eng.* **15**, 025001 (2018).
38. Matsushita, K. et al. A fully implantable wireless ECoG 128-channel recording device for human brain–machine interfaces: W-HERBS. *Front. Neurosci.* **12**, 511 (2018).
39. Wentz, C. T. et al. A wirelessly powered and controlled device for optical neural control of freely-behaving animals. *J. Neural Eng.* **8**, 046021 (2011).
40. Gutruf, P. et al. Wireless, battery-free fully implantable multimodal and multisite pace makers for applications in small animal models. *Nat. Commun.* **10**, 5742 (2019).
41. Burton, A. et al. Wireless battery-free subdermally implantable photometry systems for chronic recording of neural dynamics. *Proc. Natl Acad. Sci. USA* **117**, 2835–2845 (2020).
42. Ferguson, J. E. & Redish, A. D. Wireless communication with implanted medical devices using the conductive properties of the body. *Expert Rev. Med. Devices* **8**, 427–433 (2011).
43. Ledet, E. H., Liddle, B., Kradinova, K. & Harper, S. Smart implants in orthopedic surgery, improving patient outcomes: a review. *Innov. Entrep. Health* **5**, 41–51 (2018).
44. Yang, W., Khan, W., Wu, J. & Li, W. Single-channel opto-neurostimulators: a review. *J. Micromech. Microeng.* **29**, 043001 (2019).
45. Boyden, E. S., Zhang, F., Bamberg, E., Nagel, G. & Deisseroth, K. Millisecond-timescale, genetically targeted optical control of neural activity. *Nat. Neurosci.* **8**, 1263–1268 (2005).
46. Deisseroth, K. Optogenetics. *Nat. Methods* **8**, 26–29 (2011).
47. Pisanello, F. et al. Dynamic illumination of spatially restricted or large brain volumes via a single tapered optical fiber. *Nat. Neurosci.* **20**, 1180–1188 (2017).
48. Canales, A. et al. Multifunctional fibers for simultaneous optical, electrical and chemical interrogation of neural circuits in vivo. *Nat. Biotechnol.* **33**, 277–284 (2015).
49. Gunaydin, L. A. et al. Natural neural projection dynamics underlying social behavior. *Cell* **157**, 1535–1551 (2014).
50. Kim, C. K. et al. Simultaneous fast measurement of circuit dynamics at multiple sites across the mammalian brain. *Nat. Methods* **13**, 325–328 (2016).
51. Piatkevich, K. D. et al. A robotic multidimensional directed evolution approach applied to fluorescent voltage reporters. *Nat. Chem. Biol.* **14**, 352–360 (2018).
52. Pisano, F. et al. Depth-resolved fiber photometry with a single tapered optical fiber implant. *Nat. Methods* **16**, 1185–1192 (2019).
53. Wu, F. et al. Monolithically integrated μLEDs on silicon neural probes for high-resolution optogenetic studies in behaving animals. *Neuron* **88**, 1136–1148 (2015).
54. Ghosh, K. K. et al. Miniaturized integration of a fluorescence microscope. *Nat. Methods* **8**, 871–878 (2011).
55. Resendez, S. L. et al. Visualization of cortical, subcortical and deep brain neural circuit dynamics during naturalistic mammalian behavior with head-mounted microscopes and chronically implanted lenses. *Nat. Protoc.* **11**, 566–597 (2016).
56. Minev, I. R. et al. Electronic dura mater for long-term multimodal neural interfaces. *Science* **347**, 159–163 (2015).
57. Gilletti, A. & Muthuswamy, J. Brain micromotion around implants in the rodent somatosensory cortex. *J. Neural Eng.* **3**, 189–195 (2006).
58. Sridharan, A., Rajan, S. D. & Muthuswamy, J. Long-term changes in the material properties of brain tissue at the implant–tissue interface. *J. Neural Eng.* **10**, 066001 (2013).
59. Fan, D. et al. A wireless multi-channel recording system for freely behaving mice and rats. *PLoS ONE* **6**, e22033 (2011).
60. Lu, L. et al. Wireless optoelectronic photometers for monitoring neuronal dynamics in the deep brain. *Proc. Natl Acad. Sci. USA* **115**, E1374–E1383 (2018).
61. Zhou, A. et al. A wireless and artefact-free 128-channel neuromodulation device for closed-loop stimulation and recording in non-human primates. *Nat. Biomed. Eng.* **3**, 15–26 (2018).
62. Zhang, Y. et al. Battery-free, lightweight, injectable microsystem for in vivo wireless pharmacology and optogenetics. *Proc. Natl Acad. Sci. USA* **116**, 21427–21437 (2019).
63. Zhang, W. & Yartsev, M. M. Correlated neural activity across the brains of socially interacting bats. *Cell* **178**, 413–428.e22 (2019).
64. Jurgens, U. & Hage, S. R. Telemetric recording of neuronal activity. *Methods* **38**, 195–201 (2006).
65. Stoodley, C. J. et al. Altered cerebellar connectivity in autism and cerebellar-mediated rescue of autism-related behaviors in mice. *Nat. Neurosci.* **20**, 1744–1751 (2017).
66. Wyart, C. et al. Optogenetic dissection of a behavioural module in the vertebrate spinal cord. *Nature* **461**, 407–410 (2009).
67. Endo, H. et al. Wireless enzyme sensor system for real-time monitoring of blood glucose levels in fish. *Biosens. Bioelectron.* **24**, 1417–1423 (2009).
68. Michael, Y. M. & Ulanovsky, N. Representation of three-dimensional space in the hippocampus of flying bats. *Science* **340**, 367–372 (2013).
69. Roberts, T. F., Gobes, S. M., Murugan, M., Olveczky, B. P. & Mooney, R. Motor circuits are required to encode a sensory model for imitative learning. *Nat. Neurosci.* **15**, 1454–1459 (2012).
70. Kouhani, M. H. M., Luo, R., Madi, F., Weber, A. J. & Li, W. A wireless smartphone controlled, battery powered, head mounted light delivery system for optogenetic stimulation. In *Proc. 2018 40th Annual International Conference of the IEEE Engineering in Medicine and Biology Society (EMBC)* 3366–3369 (IEEE, 2018).
71. Gagnon-Turcotte, G. et al. A wireless headstage for combined optogenetics and multichannel electrophysiological recording. *IEEE Trans. Biomed. Circuits Syst.* **11**, 1–14 (2017).
72. Gutruf, P., Good, C. H. & Rogers, J. A. Perspective: implantable optical systems for neuroscience research in behaving animal models—current approaches and future directions. *APL Photonics* **3**, 120901 (2018).
73. Lacour, S. P., Courtine, G. & Guck, J. Materials and technologies for soft implantable neuroprostheses. *Nat. Rev. Mater.* **1**, 16063 (2016).
74. Chen, R., Canales, A. & Anikeeva, P. Neural recording and modulation technologies. *Nat. Rev. Mater.* **2**, 16093 (2017).
75. Kozai, T. D. Y., Jaquins-Gerstl, A. S., Vazquez, A. L., Michael, A. C. & Cui, X. T. Brain tissue responses to neural implants impact signal sensitivity and intervention strategies. *ACS Chem. Neurosci.* **6**, 48–67 (2015).
76. Salatino, J. W., Ludwig, K. A., Kozai, T. D. Y. & Purcell, E. K. Glial responses to implanted electrodes in the brain. *Nat. Biomed. Eng.* **1**, 862–877 (2017).
77. Rogers, J. A., Someya, T. & Huang, Y. G. Materials and mechanics for stretchable electronics. *Science* **327**, 1603–1607 (2010).
78. Veiseh, O. et al. Size- and shape-dependent foreign body immune response to materials implanted in rodents and non-human primates. *Nat. Mater.* **14**, 643–651 (2015).
79. Schiavone, G. & Lacour, S. P. Conformable bioelectronic interfaces: mapping the road ahead. *Sci. Transl. Med.* **11**, eaaw5858 (2019).
80. Vitale, F. et al. Fluidic microactuation of flexible electrodes for neural recording. *Nano Lett.* **18**, 326–335 (2018).
81. Du, Z. J. et al. Ultrasoft microwire neural electrodes improve chronic tissue integration. *Acta Biomater.* **53**, 46–58 (2017).
82. Luan, L. et al. Ultraflexible nanoelectronic probes form reliable, glial scar-free neural integration. *Sci. Adv.* **3**, e1601966 (2017).
83. Sekitani, T. & Someya, T. Stretchable, large-area organic electronics. *Adv. Mater.* **22**, 2228–2246 (2010).
84. Kim, D. H., Xiao, J. L., Song, J. Z., Huang, Y. G. & Rogers, J. A. Stretchable, curvilinear electronics based on inorganic materials. *Adv. Mater.* **22**, 2108–2124 (2010).
85. Oh, J. Y. et al. Intrinsically stretchable and healable semiconducting polymer for organic transistors. *Nature* **539**, 411–415 (2016).
86. Kaltenbrunner, M. et al. An ultra-lightweight design for imperceptible plastic electronics. *Nature* **499**, 458–463 (2013).
87. Jang, H. et al. Graphene-based flexible and stretchable electronics. *Adv. Mater.* **28**, 4184–4202 (2016).
88. Wang, S. H. et al. Skin electronics from scalable fabrication of an intrinsically stretchable transistor array. *Nature* **555**, 83–88 (2018).
89. Sun, Y. G., Choi, W. M., Jiang, H. Q., Huang, Y. G. Y. & Rogers, J. A. Controlled buckling of semiconductor nanoribbons for stretchable electronics. *Nat. Nanotechnol.* **1**, 201–207 (2006).
90. Zhang, Y. H. et al. Mechanics of ultra-stretchable self-similar serpentine interconnects. *Acta Mater.* **61**, 7816–7827 (2013).
91. Qiang, Y. et al. Transparent arrays of bilayer-nanomesh microelectrodes for simultaneous electrophysiology and two-photon imaging in the brain. *Sci. Adv.* **4**, eaat0626 (2018).
92. de la Oliva, N., Mueller, M., Stieglitz, T., Navarro, X. & del Valle, J. On the use of parylene C polymer as substrate for peripheral nerve electrodes. *Sci. Rep.* **8**, 5965 (2018).
93. Chiang, C. H. et al. Development of a neural interface for high-definition, long-term recording in rodents and nonhuman primates. *Sci. Transl. Med.* **12**, eaay4682 (2020).

94. Viventi, J. et al. Flexible, foldable, actively multiplexed, high-density electrode array for mapping brain activity in vivo. *Nat. Neurosci.* **14**, 1599–1605 (2011).
95. Xu, S. et al. Soft microfluidic assemblies of sensors, circuits, and radios for the skin. *Science* **344**, 70–74 (2014).
96. Kim, D.-H. et al. Epidermal electronics. *Science* **333**, 838–843 (2011).
97. Lee, S. et al. Ultrasoft electronics to monitor dynamically pulsing cardiomyocytes. *Nat. Nanotechnol.* **14**, 156–160 (2019).
98. Park, S. I. et al. Soft, stretchable, fully implantable miniaturized optoelectronic systems for wireless optogenetics. *Nat. Biotechnol.* **33**, 1280–1286 (2015).
99. Kim, T. I. et al. Injectable, cellular-scale optoelectronics with applications for wireless optogenetics. *Science* **340**, 211–216 (2013).
100. Shin, G. et al. Flexible near-field wireless optoelectronics as subdermal implants for broad applications in optogenetics. *Neuron* **93**, 509–521 (2017).
101. Park, S. I. et al. Stretchable multichannel antennas in soft wireless optoelectronic implants for optogenetics. *Proc. Natl Acad. Sci. USA* **113**, E8169–E8177 (2016).
102. Gutruf, P. et al. Fully implantable optoelectronic systems for battery-free, multimodal operation in neuroscience research. *Nat. Electron.* **1**, 652–660 (2018).
103. Xu, S. et al. Stretchable batteries with self-similar serpentine interconnects and integrated wireless recharging systems. *Nat. Commun.* **4**, 1543 (2013).
104. Kim, J. et al. Epidermal electronics with advanced capabilities in near-field communication. *Small* **11**, 906–912 (2015).
105. Kim, D. H., Ghaffari, R., Lu, N. S. & Rogers, J. A. Flexible and stretchable electronics for biointegrated devices. *Annu. Rev. Biomed. Eng.* **14**, 113–128 (2012).
106. Kang, S. K. et al. Bioresorbable silicon electronic sensors for the brain. *Nature* **530**, 71–76 (2016).
107. Scholten, K. & Meng, E. A review of implantable biosensors for closed-loop glucose control and other drug delivery applications. *Int. J. Pharm.* **544**, 319–334 (2018).
108. Scholten, K. & Meng, E. Materials for microfabricated implantable devices: a review. *Lab Chip* **15**, 4256–4272 (2015).
109. Hassler, C., Boretius, T. & Stieglitz, T. Polymers for neural implants. *J. Polym. Sci. Polym. Phys.* **49**, 18–33 (2011).
110. Joung, Y. H. Development of implantable medical devices: from an engineering perspective. *Int. Neurourol. J.* **17**, 98–106 (2013).
111. Fang, H. et al. Ultrathin, transferred layers of thermally grown silicon dioxide as biofluid barriers for biointegrated flexible electronic systems. *Proc. Natl Acad. Sci. USA* **113**, 11682–11687 (2016).
112. Song, E., Li, J. & Rogers, J. A. Barrier materials for flexible bioelectronic implants with chronic stability—current approaches and future directions. *APL Mater.* **7**, 050902 (2019).
113. Hashimoto, M., Hata, A., Miyata, T. & Hirase, H. Programmable wireless light-emitting diode stimulator for chronic stimulation of optogenetic molecules in freely moving mice. *Neurophotonics* **1**, 011002 (2014).
114. Gagnon-Turcotte, G. et al. A wireless optogenetic headstage with multichannel electrophysiological recording capability. *Sensors* **15**, 22776–22797 (2015).
115. Mei, H. & Irazoqui, P. P. Miniaturizing wireless implants. *Nat. Biotechnol.* **32**, 1008–1010 (2014).
116. Ben Amar, A., Kouki, A. B. & Cao, H. Power approaches for implantable medical devices. *Sensors* **15**, 28889–28914 (2015).
117. Wang, J., He, T. & Lee, C. Development of neural interfaces and energy harvesters towards self-powered implantable systems for healthcare monitoring and rehabilitation purposes. *Nano Energy* **65**, 104039 (2019).
118. Hwang, G.-T. et al. Self-powered deep brain stimulation via a flexible PIMNT energy harvester. *Energy Environ. Sci.* **8**, 2677–2684 (2015).
119. Yao, G. et al. Effective weight control via an implanted self-powered vagus nerve stimulation device. *Nat. Commun.* **9**, 5349 (2018).
120. Bullen, R. A., Arnot, T. C., Lakeman, J. B. & Walsh, F. C. Biofuel cells and their development. *Biosens. Bioelectron.* **21**, 2015–2045 (2006).
121. Settaluri, K. T., Lo, H. & Ram, R. J. Thin thermoelectric generator system for body energy harvesting. *J. Electron. Mater.* **41**, 984–988 (2012).
122. Montgomery, K. L. et al. Wirelessly powered, fully internal optogenetics for brain, spinal and peripheral circuits in mice. *Nat. Methods* **12**, 969–974 (2015).
123. Lee, S. et al. A 250 μm × 57 μm microscale opto-electronically transduced electrodes (MOTEs) for neural recording. *IEEE Trans. Biomed. Circuits Syst.* **12**, 1256–1266 (2018).
124. Ding, H. et al. Microscale optoelectronic infrared-to-visible upconversion devices and their use as injectable light sources. *Proc. Natl Acad. Sci. USA* **115**, 6632–6637 (2018).
125. Charthad, J., Weber, M. J., Chang, T. C. & Arbabian, A. A mm-sized implantable medical device (IMD) with ultrasonic power transfer and a hybrid bi-directional data link. *IEEE J. Solid State Circuits* **50**, 1741–1753 (2015).
126. Seo, D. et al. Wireless recording in the peripheral nervous system with ultrasonic neural dust. *Neuron* **91**, 529–539 (2016).
127. Rezaei, M., Maghsoudloo, E., Bories, C., De Koninck, Y. & Gosselin, B. A low-power current-reuse analog front-end for high-density neural recording implants. *IEEE Trans. Biomed. Circ. Sys.* **12**, 271–280 (2018).
128. Park, S. Y., Cho, J., Lee, K. & Yoon, E. Dynamic power reduction in scalable neural recording interface using spatiotemporal correlation and temporal sparsity of neural signals. *IEEE J. Solid State Circuits* **53**, 1102–1114 (2018).
129. Wu, X. et al. A 0.04 mm^3 16 NW wireless and batteryless sensor system with integrated Cortex-M0+ processor and optical communication for cellular temperature measurement. In *Proc. 2018 IEEE Symposium on VLSI Circuits* 191–192 (IEEE, 2018).
130. Schwarz, D. A. et al. Chronic, wireless recordings of large-scale brain activity in freely moving rhesus monkeys. *Nat. Methods* **11**, 670–676 (2014).
131. Burton, A. et al. Wireless, battery-free subdermally implantable photometry systems for chronic recording of neural dynamics. *Proc. Natl Acad. Sci. USA* **117**, 2835–2845 (2020).
132. Sivaji, V. et al. ReStore: a wireless peripheral nerve stimulation system. *J. Neurosci. Methods* **320**, 26–36 (2019).
133. Dagdeviren, C. et al. Conformal piezoelectric energy harvesting and storage from motions of the heart, lung, and diaphragm. *Proc. Natl Acad. Sci. USA* **111**, 1927–1932 (2014).
134. Ouyang, H. et al. Symbiotic cardiac pacemaker. *Nat. Commun.* **10**, 1821 (2019).
135. Falk, M., Villarrubia, C. W. N., Babanova, S., Atanassov, P. & Shleev, S. Biofuel cells for biomedical applications: colonizing the animal kingdom. *ChemPhysChem* **14**, 2045–2058 (2013).
136. Rapoport, B. I., Kedzierski, J. T. & Sarpeshkar, R. A glucose fuel cell for implantable brain–machine interfaces. *PLoS ONE* **7**, e38436 (2012).
137. Mercier, P. P., Lysaght, A. C., Bandyopadhyay, S., Chandrakasan, A. P. & Stankovic, K. M. Energy extraction from the biologic battery in the inner ear. *Nat. Biotechnol.* **30**, 1240–1243 (2012).
138. Schroeder, T. B. H. et al. An electric-eel-inspired soft power source from stacked hydrogels. *Nature* **552**, 214–218 (2017).
139. Nan, K. W. et al. Compliant and stretchable thermoelectric coils for energy harvesting in miniature flexible devices. *Sci. Adv.* **4**, eaau5859 (2018).
140. Kim, A., Ochoa, M., Rahimi, R. & Ziaie, B. New and emerging energy sources for implantable wireless microdevices. *IEEE Access* **3**, 89–98 (2015).
141. Mickle, A. D. et al. A wireless closed-loop system for optogenetic peripheral neuromodulation. *Nature* **565**, 361–365 (2019).
142. Obaid, S. & Lu, L. Highly efficient microscale gallium arsenide solar cell arrays as optogenetic power options. *IEEE Photonics J.* **11**, 8400108 (2019).
143. Zhang, H. et al. Wiress, battery-free optoelectronic systems as subdermal implants for local tissue oximetry. *Sci. Adv.* **5**, eaaw0873 (2019).
144. Zhang, Y. et al. Battery-free, fully implantable optofluidic cuff system for wireless optogenetic and pharmacological neuromodulation of peripheral nerves. *Sci. Adv.* **5**, eaaw5296 (2019).
145. Jia, Y. Y., Wang, Z. Y., Mirbozorgi, S. A. & Ghovanloo, M. A closed-loop wireless homecage for optogenetic stimulation experiments. In *Proc. 2015 IEEE Biomedical Circuits and Systems Conference (BioCAS)* 426–429 (2015).
146. Khalifa, A. et al. The Microbead: a 0.009 mm^3 implantable wireless neural stimulator. *IEEE Trans. Biomed. Circuits Syst.* **13**, 971–985 (2019).
147. Dagdeviren, C. et al. Flexible piezoelectric devices for gastrointestinal motility sensing. *Nat. Biomed. Eng.* **1**, 807–817 (2017).
148. Dagdeviren, C. et al. Recent progress in flexible and stretchable piezoelectric devices for mechanical energy harvesting, sensing and actuation. *Extrem. Mech. Lett.* **9**, 269–281 (2016).
149. El Ichi-Ribault, S. et al. Remote wireless control of an enzymatic biofuel cell implanted in a rabbit for 2 months. *Electrochim. Acta* **269**, 360–366 (2018).
150. Dong, K. et al. Microbial fuel cell as power supply for implantable medical devices: a novel configuration design for simulating colonic environment. *Biosens. Bioelectron.* **41**, 916–919 (2013).
151. Gonzalez-Solino, C. & Lorenzo, M. D. Enzymatic fuel cells: towards self-powered implantable and wearable diagnostics. *Biosensors* **8**, 11 (2018).
152. Rasmussen, M., Ritzmann, R. E., Lee, I., Pollack, A. J. & Scherson, D. An implantable biofuel cell for a live insect. *J. Am. Chem. Soc.* **134**, 1458–1460 (2012).
153. Halamkova, L. et al. Implanted biofuel cell operating in a living snail. *J. Am. Chem. Soc.* **134**, 5040–5043 (2012).
154. Castorena-Gonzalez, J. A. et al. Biofuel cell operating in vivo in rat. *Electroanalysis* **25**, 1579–1584 (2013).
155. Zebda, A. et al. Challenges for successful implantation of biofuel cells. *Bioelectrochemistry* **124**, 57–72 (2018).
156. Yu, X. et al. Skin-integrated wireless haptic interfaces for virtual and augmented reality. *Nature* **575**, 473–479 (2019).
157. Merli, F. et al. Design, realization and measurements of a miniature antenna for implantable wireless communication systems. *IEEE Trans. Antennas Propag.* **59**, 3544–3555 (2011).

158. Park, S. I. et al. Ultraminiaturized photovoltaic and radio frequency powered optoelectronic systems for wireless optogenetics. *J. Neural Eng.* **12**, 056002 (2015).
159. Xie, Z., Avila, R., Huang, Y. & Rogers, J. A. Flexible and stretchable antennas for biointegrated electronics. *Adv. Mater.* **32**, e1902767 (2019).
160. Dobkin, D. M. *The RF in RFID: UHF RFID in Practice* (Newnes, 2012).
161. Ho, J. S. et al. Self-tracking energy transfer for neural stimulation in untethered mice. *Phys. Rev. Appl.* **4**, 024001 (2015).
162. Elder, J. A. & Cahill, D. F. (eds) *Biological Effects of Radiofrequency Radiation* (US Environmental Protection Agency, 1984).
163. Marincic, A. S. Nikola Tesla and the wireless transmission of energy. *IEEE Trans. Power Appar. Syst.* **101**, 4064–4068 (1982).
164. Tesla, N. Apparatus for transmitting electrical energy. US Patent 1,119,732 (1914).
165. Das Barman, S., Reza, A. W., Kumar, N., Karim, M. E. & Munir, A. Wireless powering by magnetic resonant coupling: recent trends in wireless power transfer system and its applications. *Renew. Sust. Energ. Rev.* **51**, 1525–1552 (2015).
166. Sallan, J., Villa, J. L., Llombart, A. & Sanz, J. F. Optimal design of ICPT systems applied to electric vehicle battery charge. *IEEE Trans. Ind. Electron.* **56**, 2140–2149 (2009).
167. Kalwar, K. A., Aamir, M. & Mekhilef, S. Inductively coupled power transfer (ICPT) for electric vehicle charging—a review. *Renew. Sust. Energ. Rev.* **47**, 462–475 (2015).
168. Fareq, M., Fitra, M., Irwanto, M., Hasan, S. & Arinal, M. Low wireless power transfer using inductive coupling for mobile phone charger. *J. Phys. Conf. Ser.* **495**, 012019 (2014).
169. Kurs, A. et al. Wireless power transfer via strongly coupled magnetic resonances. *Science* **317**, 83–86 (2007).
170. Ho, S. L., Wang, J. H., Fu, W. N. & Sun, M. G. A comparative study between novel witricity and traditional inductive magnetic coupling in wireless charging. *IEEE Trans. Magn.* **47**, 1522–1525 (2011).
171. Low, Z. N., Chinga, R. A., Tseng, R. & Lin, J. S. Design and test of a high-power high-efficiency loosely coupled planar wireless power transfer system. *IEEE Trans. Ind. Electron.* **56**, 1801–1812 (2009).
172. Zhang, Y. M., Zhao, Z. M. & Chen, K. N. Frequency decrease analysis of resonant wireless power transfer. *IEEE Trans. Power Electron.* **29**, 1058–1063 (2014).
173. Yoon, I. J. & Ling, H. Investigation of near-field wireless power transfer in the presence of lossy dielectric materials. *IEEE Trans. Antennas Propag.* **61**, 482–488 (2013).
174. Poon, A. S. Y., O'Driscoll, S. & Meng, T. H. Optimal frequency for wireless power transmission into dispersive tissue. *IEEE Trans. Antennas Propag.* **58**, 1739–1750 (2010).
175. Cecil, S. et al. Numerical assessment of specific absorption rate in the human body caused by NFC devices. *In Proc. 2010 Second International Workshop on Near Field Communication* 65–70 (IEEE, 2010).
176. Chung, H. U. et al. Binodal, wireless epidermal electronic systems with in-sensor analytics for neonatal intensive care. *Science* **363**, eaau0780 (2019).
177. Kim, J. et al. Miniaturized flexible electronic systems with wireless power and near-field communication capabilities. *Adv. Funct. Mater.* **25**, 4761–4767 (2015).
178. Lazaro, A., Villarino, R. & Girbau, D. A survey of NFC sensors based on energy harvesting for IoT applications. *Sensors* **18**, 3746 (2018).
179. Ray, T. R. et al. Bio-integrated wearable systems: a comprehensive review. *Chem. Rev.* **119**, 5461–5533 (2019).
180. Hui, S. Y. R., Zhong, W. & Lee, C. K. A critical review of recent progress in mid-range wireless power transfer. *IEEE Trans. Power Electron.* **29**, 4500–4511 (2014).
181. Denisov, A. & Yeatman, E. Ultrasonic vs. inductive power delivery for miniature biomedical implants. In *Proc. 2010 International Conference on Body Sensor Networks* 84–89 (IEEE, 2010).
182. Podgorski, K. & Ranganathan, G. Brain heating induced by near-infrared lasers during multiphoton microscopy. *J. Neurophysiol.* **116**, 1012–1023 (2016).
183. Mialhe, P., & Mouhamed, S. & Haydar, A. The solar cell output power dependence on the angle of incident radiation. *Renew. Energ.* **1**, 519–521 (1991).
184. Johnson, B. C. et al. StimDust: a 6.5 mm^3, wireless ultrasonic peripheral nerve stimulator with 82% peak chip efficiency. In *Proc. 2018 IEEE Custom Integrated Circuits Conference (CICC)* 1–4 (IEEE, 2018).
185. Piech, D. K. et al. A wireless millimetre-scale implantable neural stimulator with ultrasonically powered bidirectional communication. *Nat. Biomed. Eng.* **4**, 207–222 (2020).
186. Basaeri, H., Christensen, D. B. & Roundy, S. A review of acoustic power transfer for bio-medical implants. *Smart Mater. Struct.* **25**, 123001 (2016).
187. Seo, D. et al. Ultrasonic beamforming system for interrogating multiple implantable sensors. In *Proc. 37th Annual International Conference of the IEEE Engineering in Medicine and Biology Society* 2673–2676 (IEEE, 2015).
188. *Information for Manufacturers Seeking Marketing Clearance of Diagnostic Ultrasound Systems and Transducers* (US Food and Drug Administration, 2008).
189. O'Brien, W. D. Jr. Ultrasound-biophysics mechanisms. *Prog. Biophys. Mol. Biol.* **93**, 212–255 (2007).
190. Bushberg, J. T. & Boone, J. M. *The Essential Physics of Medical Imaging* (Lippincott Williams & Wilkins, 2011).
191. Nelson, T. R., Fowlkes, J. B., Abramowicz, J. S. & Church, C. C. Ultrasound biosafety considerations for the practicing sonographer and sonologist. *J. Ultrasound Med.* **28**, 139–150 (2009).
192. Samineni, V. K. et al. Fully implantable, battery-free wireless optoelectronic devices for spinal optogenetics. *Pain* **158**, 2108–2116 (2017).
193. Harvey, C. D., Collman, F., Dombeck, D. A. & Tank, D. W. Intracellular dynamics of hippocampal place cells during virtual navigation. *Nature* **461**, 941–946 (2009).
194. Tye, K. M. et al. Amygdala circuitry mediating reversible and bidirectional control of anxiety. *Nature* **471**, 358–362 (2011).
195. Yilmaz, G. & Dehollain, C. *Wireless Power Transfer and Data Communication for Neural Implants. Case Study: Epilepsy Monitoring* (Springer, 2017).
196. Liang, T. & Yuan, Y. J. Wearable medical monitoring systems based on wireless networks: a review. *IEEE Sens. J.* **16**, 8186–8199 (2016).
197. Zhang, Z. H., Russell, L. E., Packer, A. M., Gauld, O. M. & Hausser, M. Closed-loop all-optical interrogation of neural circuits in vivo. *Nat. Methods* **15**, 1037–1040 (2018).
198. Mirza, K. B., Golden, C. T., Nikolic, K. & Toumazou, C. Closed-loop implantable therapeutic neuromodulation systems based on neurochemical monitoring. *Front. Neurosci.* **13**, 808 (2019).
199. Jun, J. J. et al. Fully integrated silicon probes for high-density recording of neural activity. *Nature* **551**, 232–236 (2017).
200. Aravanis, A. M. et al. An optical neural interface: in vivo control of rodent motor cortex with integrated fiberoptic and optogenetic technology. *J. Neural Eng.* **4**, S143–S156 (2007).
201. Shin, Y. et al. Characterization of fiber-optic light delivery and light-induced temperature changes in a rodent brain for precise optogenetic neuromodulation. *Biomed. Opt. Express* **7**, 4450–4471 (2016).
202. Wang, Z., Hu, M., Ai, X., Zhang, Z. & Xing, B. Near-infrared manipulation of membrane ion channels via upconversion optogenetics. *Adv. Biosyst.* **3**, e1800233 (2019).
203. Lin, J. Y., Knutsen, P. M., Muller, A., Kleinfeld, D. & Tsien, R. Y. ReaChR: a red-shifted variant of channelrhodopsin enables deep transcranial optogenetic excitation. *Nat. Neurosci.* **16**, 1499–1508 (2013).
204. Arrenberg, A. B., Bene, F. D. & Baier, H. Optical control of zebrafish behavior with halorhodopsin. *Proc. Natl Acad. Sci. USA* **106**, 17968–17973 (2009).
205. Yarmolenko, P. S. et al. Thresholds for thermal damage to normal tissues: an update. *Int. J. Hyperth.* **27**, 320–343 (2011).
206. Goncalves, S. B. et al. LED optrode with integrated temperature sensing for optogenetics. *Micromachines* **9**, 473 (2018).
207. Khan, W. et al. Inductively coupled, mm-sized, single channel optical neuro-stimulator with intensity enhancer. *Microsyst. Nanoeng.* **5**, 23 (2019).
208. Kampasi, K. et al. Fiberless multicolor neural optoelectrode for in vivo circuit analysis. *Sci. Rep.* **6**, 30961 (2016).
209. Samineni, V. K. et al. Optogenetic silencing of nociceptive primary afferents reduces evoked and ongoing bladder pain. *Sci. Rep.* **7**, 15865 (2017).
210. Busskamp, V. & Roska, B. Optogenetic approaches to restoring visual function in retinitis pigmentosa. *Curr. Opin. Neurobiol.* **21**, 942–946 (2011).
211. Busskamp, V., Picaud, S., Sahel, J. A. & Roska, B. Optogenetic therapy for retinitis pigmentosa. *Gene. Ther.* **19**, 169–175 (2012).
212. Chow, B. Y. & Boyden, E. S. Optogenetics and translational medicine.*Sci. Transl. Med.* **5**, 177ps175 (2013).
213. Krook-Magnuson, E., Armstrong, C., Oijala, M. & Soltesz, I. On-demand optogenetic control of spontaneous seizures in temporal lobe epilepsy. *Nat. Commun.* **4**, 1376 (2013).
214. Paz, J. T. et al. Closed-loop optogenetic control of thalamus as a tool for interrupting seizures after cortical injury. *Nat. Neurosci.* **16**, 64–70 (2013).
215. Nussinovitch, U. & Gepstein, L. Optogenetics for in vivo cardiac pacing and resynchronization therapies. *Nat. Biotechnol.* **33**, 750–754 (2015).
216. Shao, J. et al. Smartphone-controlled optogenetically engineered cells enable semiautomatic glucose homeostasis in diabetic mice. *Sci. Transl. Med.* **9**, eaal2298 (2017).
217. Bansal, A., Yang, F., Xi, T., Zhang, Y. & Ho, J. S. In vivo wireless photonic photodynamic therapy. *Proc. Natl Acad. Sci. USA* **115**, 1469–1474 (2018).
218. Kramer, R. H., Mourot, A. & Adesnik, H. Optogenetic pharmacology for control of native neuronal signaling proteins. *Nat. Neurosci.* **16**, 816–823 (2013).
219. Banghart, M. R. & Sabatini, B. L. Photoactivatable neuropeptides for spatiotemporally precise delivery of opioids in neural tissue. *Neuron* **73**, 249–259 (2012).

220. Jennings, J. H. et al. Distinct extended amygdala circuits for divergent motivational states. *Nature* **496**, 224–228 (2013).
221. Stamatakis, A. M. et al. A unique population of ventral tegmental area neurons inhibits the lateral habenula to promote reward. *Neuron* **80**, 1039–1053 (2013).
222. McCall, J. G. et al. CRH engagement of the locus coeruleus noradrenergic system mediates stress-induced anxiety. *Neuron* **87**, 605–620 (2015).
223. McCall, J. G. et al. Preparation and implementation of optofluidic neural probes for in vivo wireless pharmacology and optogenetics. *Nat. Protoc.* **12**, 219–237 (2017).
224. Creed, M., Pascoli, V. J. & Lüscher, C. Refining deep brain stimulation to emulate optogenetic treatment of synaptic pathology. *Science* **347**, 659–664 (2015).
225. McCall, J. G. & Jeong, J. W. Minimally invasive probes for programmed microfluidic delivery of molecules in vivo. *Curr. Opin. Neurobiol.* **36**, 78–85 (2017).
226. Noh, K. N. et al. Miniaturized, battery-free optofluidic systems with potential for wireless pharmacology and optogenetics. *Small* **14**, 1702479 (2018).
227. Shmuel, A., Augath, M., Oeltermann, A. & Logothetis, N. K. Negative functional MRI response correlates with decreases in neuronal activity in monkey visual area V1. *Nat. Neurosci.* **9**, 569–577 (2006).
228. Liu, J. N., Bu, W. & Shi, J. Chemical design and synthesis of functionalized probes for imaging and treating tumor hypoxia. *Chem. Rev.* **117**, 6160–6224 (2017).
229. Hopf, H. W. & Rollins, M. D. Wounds: an overview of the role of oxygen. *Antioxid. Redox Signal.* **9**, 1183–1192 (2007).
230. Neely, R. M., Piech, D. K., Santacruz, S. R., Maharbiz, M. M. & Carmena, J. M. Recent advances in neural dust: towards a neural interface platform. *Curr. Opin. Neurobiol.* **50**, 64–71 (2018).
231. Ghanbari, M. M. et al. A sub-mm^3 ultrasonic free-floating implant for multi-mote neural recording. *IEEE J. Solid State Circuits* **54**, 3017–3030 (2019).
232. Ghanbari, M. M. et al. A 0.8 mm^3 ultrasonic implantable wireless neural recording system with linear AM backscattering. In *Proc. 2019 IEEE International Solid-State Circuits Conference (ISSCC)* 284–286 (2019).
233. Kang, S. K., Koo, J., Lee, Y. K. & Rogers, J. A. Advanced materials and devices for bioresorbable electronics. *Acc. Chem. Res.* **51**, 988–998 (2018).
234. Won, S. M. et al. Natural wax for transient electronics. *Adv. Funct. Mater.* **28**, e1801819 (2018).
235. Boutry, C. M. et al. Biodegradable and flexible arterial-pulse sensor for the wireless monitoring of blood flow. *Nat. Biomed. Eng.* **3**, 47–57 (2019).
236. Koo, J. et al. Wireless bioresorbable electronic system enables sustained nonpharmacological neuroregenerative therapy. *Nat. Med.* **24**, 1830–1836 (2018).
237. Son, D. et al. Bioresorbable electronic stent integrated with therapeutic nanoparticles for endovascular diseases. *ACS Nano* **9**, 5937–5946 (2015).
238. Pashaie, R. et al. Closed-loop optogenetic brain interface. *IEEE Trans. Biomed. Eng.* **62**, 2327–2337 (2015).
239. Jonsson, A. et al. Bioelectronic neural pixel: chemical stimulation and electrical sensing at the same site. *Proc. Natl Acad. Sci. USA* **113**, 9440–9445 (2016).
240. Capogrosso, M. et al. A brain–spine interface alleviating gait deficits after spinal cord injury in primates. *Nature* **539**, 284–288 (2016).
241. Zanos, S. Closed-loop neuromodulation in physiological and translational research. *Cold Spring Harb. Perspect. Med.* **9**, a034314 (2019).
242. Lo, M. C. & Widge, A. S. Closed-loop neuromodulation systems: next-generation treatments for psychiatric illness. *Int. Rev. Psychiatry* **29**, 191–204 (2017).

Acknowledgements

L.C. and P.G. acknowledge the support of the Improving Health TRIF Project. P.G. acknowledges the support of NIG-NINDS R01NS112535 and start-up funds from the Department of Biomedical Engineering at the University of Arizona. S.M.W. acknowledges the support of the MSIT (Ministry of Science and ICT), Korea, under the ICT Creative Consilience program (IITP-2020-0-01821), supervised by the IITP (Institute for Information & communications Technology Planning & Evaluation). S.M.W. acknowledges support by a National Research Foundation of Korea (NRF) grant funded by the Korea government (MSIP; Ministry of Science, ICT & Future Planning; grant no. 2020R1G1A1101267). S.M.W. acknowledges the support by Nano Material Technology Development Program (2020M3H4A1A03084600) through the National Research Foundation of Korea (NRF) funded by the Ministry of Science and ICT of Korea.

Author contributions

All authors contributed to writing and revising the manuscript, and approved the final version.

Competing interests

The authors declare no competing interests.

Additional information

Correspondence should be addressed to P.G. or J.A.R.